Article

Cell Chemical Biology

A non-reactive natural product precursor of the duocarmycin family has potent and selective antimalarial activity

Graphical abstract

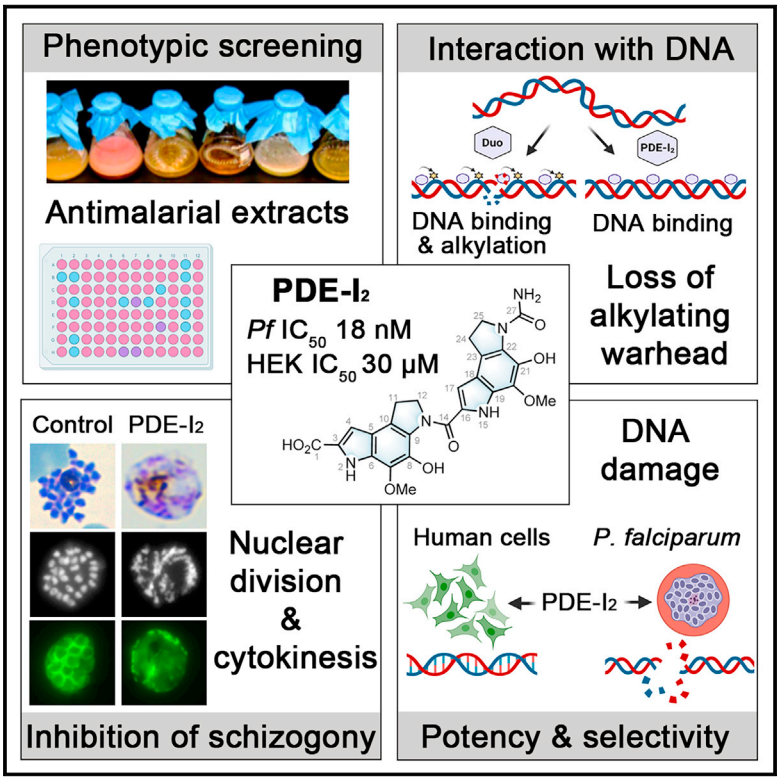

Highlights

- Antimalarial screening of an extract library identifies the natural product PDE-I_2
- PDE-I_2 is a non-toxic duocarmycin family member, lacking the alkylating warhead
- PDE-I_2 is a nanomolar inhibitor of parasite schizogony with 1,000-fold selectivity

Authors

Arne Alder, Nicole S. Struck, Min Xu, ..., Sarah Lemcke, Tim W. Gilberger, Gerard D. Wright

Correspondence

gilberger@bnitm.de (T.W.G.), wrightge@mcmaster.ca (G.D.W.)

In brief

Using a phenotypic screen of a natural product library, Alder et al. identify PDE-I_2, a potent and selective inhibitor of malaria proliferation. PDE-I_2 is a member of the anticancer duocarmycin family but lacks its DNA-modifying properties. PDE-I_2 treatment leads to malaria-specific DNA damage, impaired nuclear segregation, and arrest of cytokinesis.

Alder et al., 2022, Cell Chemical Biology *29*, 840–853
May 19, 2022
https://doi.org/10.1016/j.chembiol.2021.10.005

CellPress

CellPress

Cell Chemical Biology

Article

A non-reactive natural product precursor of the duocarmycin family has potent and selective antimalarial activity

Arne Alder,[1,2,3] Nicole S. Struck,[2,4,5] Min Xu,[4] Jarrod W. Johnson,[4] Wenliang Wang,[4] Daniel Pallant,[4] Michael A. Cook,[4] Janis Rambow,[1,2,3] Sarah Lemcke,[1,2,3] Tim W. Gilberger,[1,2,3,*] and Gerard D. Wright[4,6,*]

[1]Centre for Structural Systems Biology, 22607 Hamburg, Germany
[2]Bernhard Nocht Institute for Tropical Medicine, Department of Cellular Parasitology, 20359 Hamburg, Germany
[3]University of Hamburg, Department of Biology, 20146 Hamburg, Germany
[4]M.G. DeGroote Institute for Infectious Disease Research, Department of Biochemistry and Biomedical Sciences, McMaster University, Hamilton, ON L8N 3Z5, Canada
[5]German Centre for Infection Research (DZIF), Hamburg-Lübeck-Borstel-Riems, Hamburg, Germany
[6]Lead contact
*Correspondence: gilberger@bnitm.de (T.W.G.), wrightge@mcmaster.ca (G.D.W.)
https://doi.org/10.1016/j.chembiol.2021.10.005

SUMMARY

We identify a selective nanomolar inhibitor of blood-stage malarial proliferation from a screen of microbial natural product extracts. The responsible compound, PDE-I_2, is a precursor of the anticancer duocarmycin family that preserves the class's sequence-specific DNA binding but lacks its signature DNA alkylating cyclopropyl warhead. While less active than duocarmycin, PDE-I_2 retains comparable antimalarial potency to chloroquine. Importantly, PDE-I_2 is >1,000-fold less toxic to human cell lines than duocarmycin, with mitigated impacts on eukaryotic chromosome stability. PDE-I_2 treatment induces severe defects in parasite nuclear segregation leading to impaired daughter cell formation during schizogony. Time-of-addition studies implicate parasite DNA metabolism as the target of PDE-I_2, with defects observed in DNA replication and chromosome integrity. We find the effect of duocarmycin and PDE-I_2 on parasites is phenotypically indistinguishable, indicating that the DNA binding specificity of duocarmycins is sufficient and the genotoxic cyclopropyl warhead is dispensable for the parasite-specific selectivity of this compound class.

INTRODUCTION

Malaria is one of the deadliest infectious diseases on the planet, responsible for 409,000 deaths and 229 million cases in 2019 (World Health Organization, 2020). Parasites of the genus *Plasmodium* are the causative agent, with the species *P. falciparum* and *P. vivax* responsible for the majority of malaria infections in humans. Those most affected are children under 5 years and pregnant women in sub-Saharan Africa (White et al., 2014a). Since 2000, prevention measures, including drug prophylaxis, improved rapid diagnostic tests, and vector control strategies, have successfully reduced worldwide malaria cases (Bhatt et al., 2015). Unfortunately, this trend has stalled over the past 5 years. The lack of an effective vaccine means that disease management is dependent on access to antimalarial drugs. Treatment of malaria is mainly based on artemisinin-based combination therapy (ACT), especially for severe malaria infections. However, resistance to almost all available drugs, including ACT, is making it increasingly difficult to manage the disease (Ashley et al., 2014). Consequently, there is a pressing need to discover and develop new antimalarial drug leads with novel modes of action.

While several new agents derived mainly from known drugs are in preclinical development or clinical trials, new chemical scaffolds are desired to minimize the risk of emerging resistance (Wells, 2011). Phenotypic screens using compound libraries help identify chemotypes with entirely new mechanisms of action (first-in-class drug candidates). In contrast to target-based strategies, phenotypic screens can simulate physiological conditions, leading to the identification of compounds with desired solubility and membrane permeability (Chatterjee and Yeung, 2012). This approach led to the identification of thousands of novel compounds with potent antiplasmodial activity and new antiplasmodial chemotypes (Gamo et al., 2010; Guiguemde et al., 2010, 2012; Plouffe et al., 2016; Spangenberg et al., 2013; Sun et al., 2017; Van Voorhis et al., 2016). One promising molecule is the spiroindolone NITD609 identified by a phenotypic screen of a Novartis library of 12,000 natural products (NPs) and synthetic compounds (Rottmann et al., 2010). The synthetic compound NITD609 and other spiroindolone derivates have been tested in human clinical trials and show rapid antiplasmodial clearance (Gaur et al., 2020; White et al., 2014b).

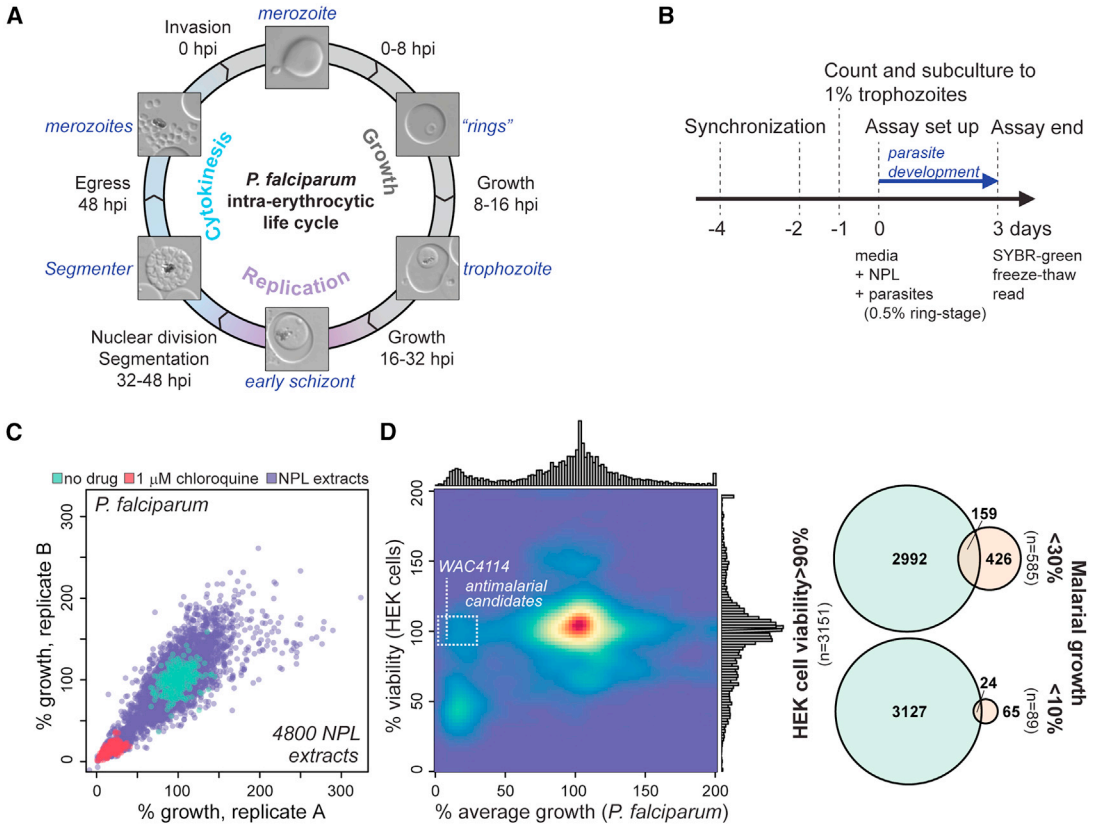

Figure 1. A screen of blood stage *P. falciparum* against a library of microbial NP extracts

(A) Schematic representation of the intraerythrocytic life cycle of *P. falciparum*. After active invasion of a RBC, the parasites develop from ring to trophozoite stage followed by the formation of daughter merozoites by schizogony. The timing of DNA replication and cytokinesis/nuclear division is indicated.

(B) Assay setup for antiplasmodial screening of NP extracts. Synchronous parasites at 0.5% ring stages were cultured in the presence of extracts for 72 hours. Parasite proliferation was determined based on SYBR Green DNA staining.

(C) Replicate *P. falciparum* screen data of 4800 NPL extracts; 1 μM chloroquine was included as a positive control. Percent growth represents assay signal, background adjusted by RBC only controls, and normalized to the average signal in the no-drug controls.

(D) (Left) One-dimensional and 2-dimensional representations of primary *P. falciparum* and secondary HEK cell viability assays. Specific candidate extracts were drawn from the indicated region. Plot was generated by kernel density estimate. Percent viability of HEK cells represents assay signal, background adjusted, and normalized to the average signal in low DMSO controls. (Right) Intersection of extracts conferring minimal effects on HEK cell viability and antimalarial activity.

NPs produced by plants and microbes offer a proven source of new antimalarial compounds. Given malaria's persistence in human history, there is a deep cultural knowledge of traditional medicines, particularly herbal remedies, for malaria treatment (Pan et al., 2018; Wells, 2011). Some of the most effective antimalarial drugs, including quinine and artemisinin, are NPs derived from such plant-based medicines. In contrast, reports of antimalarial NPs from microbial sources are uncommon, though they are proven sources of antibacterial, antifungal, and anticancer drugs (Ahmad et al., 2017; Zhang et al., 2018b).

Encouraged by the reports of small molecule phenotypic screens of malaria blood stages (Plouffe et al., 2016; Sun et al., 2017), we performed a pilot screen of our in-house library of microbial NP extracts. We report the identification of PDE-I_2, a precursor in the biosynthesis of duocarmycin anticancer compounds, as a highly selective blood-stage *P. falciparum* inhibitor with 1,000-fold selectivity toward parasite over human cells.

RESULTS

Identification of non-toxic *P. falciparum* inhibitors from a high-throughput screen of microbial natural product extracts

During normal development, a single merozoite enters a red blood cell (RBC), progresses from an early "ring" stage to a trophozoite over the course of 24 hours, then undergoes multiple rounds of DNA synthesis and asynchronous nuclear division to form a multi-nuclei schizont. The mature schizont undergoes synchronous division (the "segmenter" stage) to up to 32 progeny (Cowman et al., 2016) that are released into the bloodstream (Figure 1A). We applied a cell-based assay to identify proliferation inhibitors of *P. falciparum* using SYBR Gold DNA quantification as a proxy for parasite replication in the context of anucleate RBCs (Figure 1B) (Smilkstein et al., 2004). In this assay, parasites are seeded at the ring stage of development, mature to the schizont stage, and re-infect and proliferate within erythrocytes over the course of the assay, leading to a >10-fold increase in

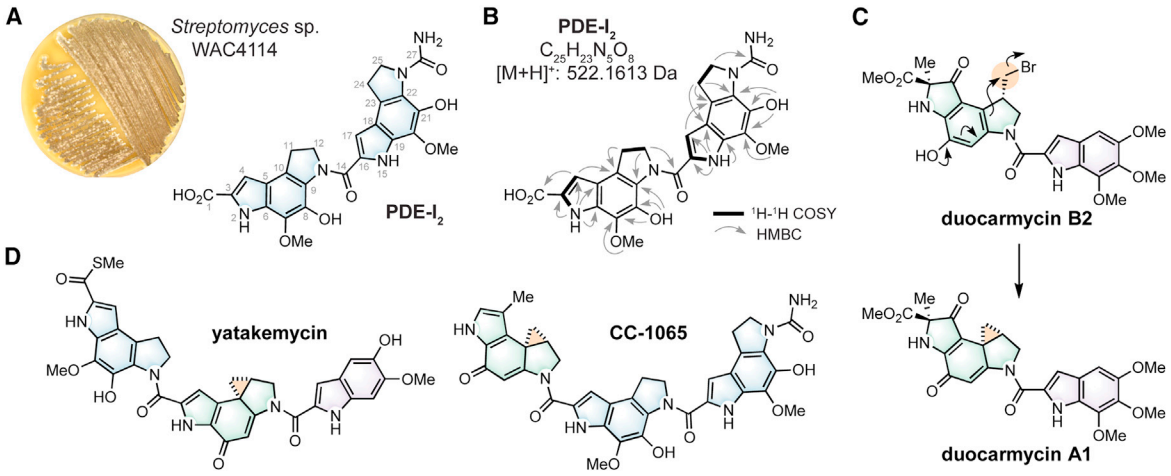

Figure 2. PDE-I_2 is an analog of the duocarmycin family

(A) Structure of PDE-I_2, purified from *Streptomyces* sp. WAC4114. Structural elements common to related compounds in (C) are indicated by colored ring systems.

(B) Annotated structure of PDE-I_2 showing NMR assignments.

(C) Certain members of the duocarmycin family initially lack a cyclopropyl-group but undergo spontaneously conversion in cells to the warhead-containing form, as shown for duocarmycin B2.

(D) Additional members of the duocarmycin family of molecules. Common structural elements are noted by colored ring systems. The reactive warhead of each molecule is highlighted by an orange circle. See also Table S1.

SYBR Gold signal (Figure 1B). The anti-proliferative effect of a known antimalarial, chloroquine, is readily distinguished from growth controls (Figure 1C). We screened 4,800 NP extracts derived from our collection of environmental bacteria and fungi, yielding a reproducible range of effects on parasite proliferation (Figure 1C). The assay showed a bimodal distribution of values with either strong suppression or minimal effects on parasite proliferation (IQR 73%–116%) (Figure 1D); 585 extracts (12%) conferred a >70% reduction and 89 (1.9%) conferred a >90% reduction of parasite proliferation.

To evaluate potential human cytotoxicity, we counter-screened our NP collection against HEK293T cells using a resazurin-based metabolic indicator of cell viability (Figure 1D). Most extracts were non-toxic with a median viability of 109% (IQR 90%–120%). To select compounds with maximal antimalarial effect and minimal toxicity for mammalian cells, only extracts with >90% inhibition against malaria parasites (N = 89) with minimal inhibitory effect on HEK cells (>90% viability, N = 3,151) were chosen for follow up (N = 24). We cultured eight of the corresponding organisms and generated extracts, of which seven yielded reproducible malarial inhibition in direct phenotype-based assays. The extract of one organism (*Streptomyces* sp. WAC4114) was the most potent, with crude fractions showing activity at dilutions suggestive of nanomolar potency, and consequently was chosen for further study in this report.

PDE-I_2, a member of the duocarmycin family lacking the reactive warhead, is the antimalarial compound from *Streptomyces* sp. WAC4114

The active antimalarial component produced by *Streptomyces* sp. WAC4114 was purified using activity-guided methods, as outlined in the STAR Methods (Figure 2A). The ESI-MS molecular ion cluster at *m/z* 522 $[M + H]^+$ and the 1D NMR spectra are consistent with the molecular formula $C_{25}H_{23}N_5O_8$ (Table S1). The ^{1}H- and ^{13}C-NMR spectra indicate the presence of two highly similar benzodipyrrole systems. The correlations from H-12 (at δ 4.66 ppm) and H-17 (at δ 7.05 ppm) to C-14 (at δ 160.7 ppm) in the HMBC spectrum are consistent with a structure wherein the two benzodipyrroles are connected through an amide bond (Figure 2B). The active compound is a symmetrical benzodipyrrole, with the two subunits differing only in the linkage of a formamide unit onto the pyrrole of the "north" side compared with a formic acid on the "south" side (Figure 2A). A search of known structures identified the compound as PDE-I_2, a pseudosymmetrical phosphodiesterase inhibitor (Enomoto et al., 1978). PDE-I_2 is an element of the potent anticancer compound CC-1065, which had previously been synthesized by Carter et al. (Carter et al., 1987) and Boger and Coleman (Boger and Coleman, 1988).

CC-1065 is a member of the duocarmycin anticancer compound family that includes other bacterial NPs such as yatakemycin (Figures 2C and 2D). These highly cytotoxic agents are characterized by one to three modified benzodipyrrole units, one of which has a cyclopropyl warhead (Boger and Johnson, 1995; Hurley et al., 1988; Parrish et al., 2003). Duocarmycins bind to the minor groove of the B form of AT-rich DNA, positioning the warhead for alkylation of an adenine at the N3 position. PDE-I_2 lacks the characteristic cyclopropyl warhead of duocarmycins and cannot alkylate DNA, the primary driver of CC-1065 toxicity.

PDE-I_2 is the product of an impaired duocarmycin biosynthetic program

PDE-I_2 was reported as a shunt product from the biosynthetic pathway of CC-1065, detected following deletion of the radical SAM (rSAM) enzyme coding gene *c10P* in *Streptomyces zelensis* NRRL11183 (Wu et al., 2017). The C10P rSAM enzyme is

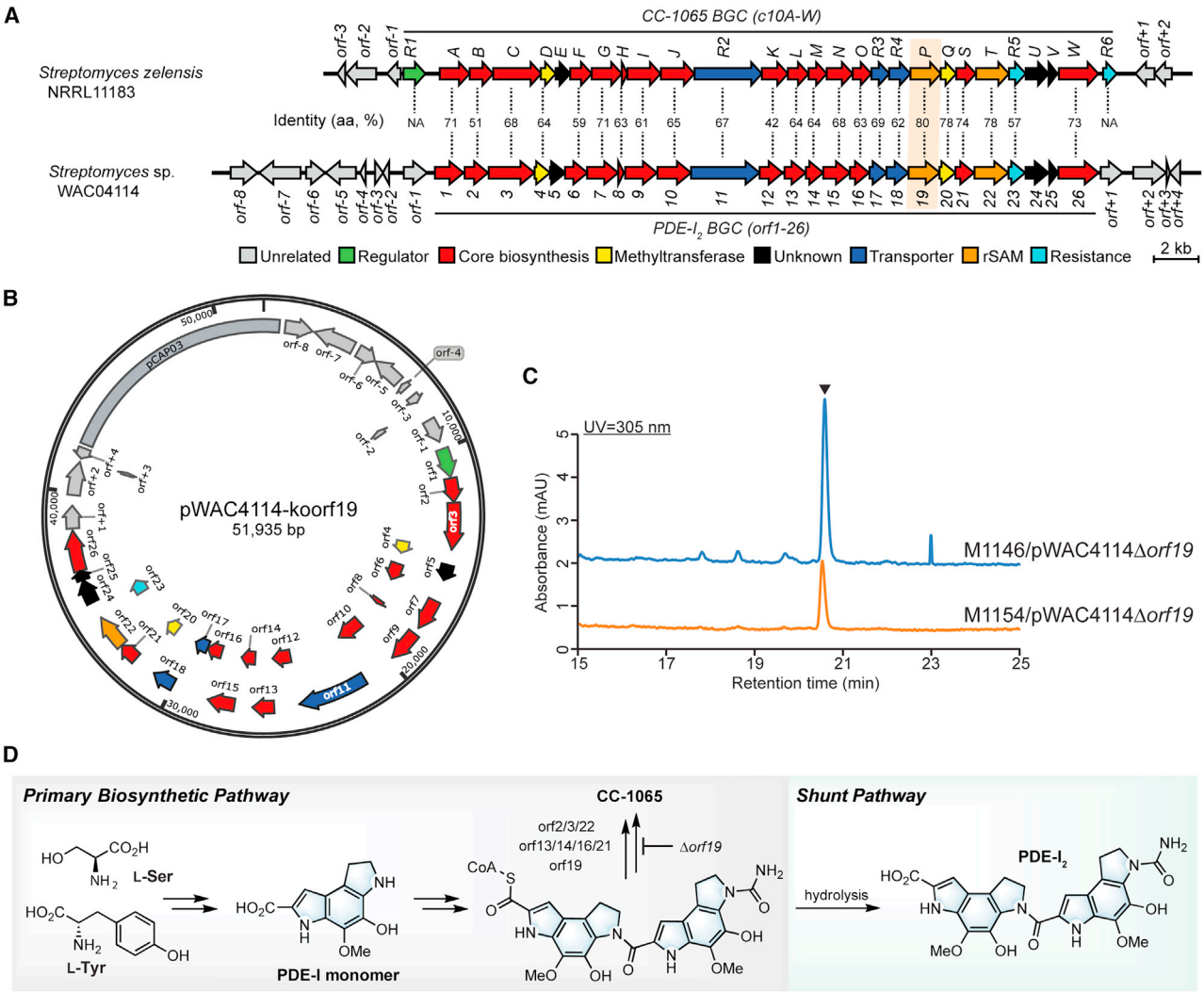

Figure 3. Characterization of the BGC of PDE-I_2 from *Streptomyces* sp. WAC4114

(A) BGC of PDE-I_2. The BGC composition of PDE-I_2 is almost identical to that of CC-1065 in *S. zelensis* NRRL11183, except for the absence of *c10R1* regulation and *c10R6* resistance genes. Amino acid identity of each protein encoded between both BGCs is shown.

(B) Captured PDE-I_2 BGC in pCAP03 using TAR. *orf19* encoding the rSAM gene was deleted through λ-red mediated recombination to direct production of PDE-I_2 in the heterologous expression system.

(C) Heterologous expression of PDE-I_2 in *S. coelicolor* M1146 and M1154. The elution peak labeled by inverted triangle identifies PDE-I_2.

(D) Proposed metabolic pathway of CC1065 synthesis (Wu et al., 2017). orf19, the ortholog of C10P, is expected to be involved in installation of the cyclopropyl group of CC-1065. PDE-I_2 is likely the hydrolysis product of the indicated intermediate in the proposed biosynthetic pathway.

necessary for the introduction of the cyclopropyl warhead during CC-1065 biosynthesis. This gene is also conserved in the biosynthesis of the benzodipyrrole family of antitumor compounds such as duocarmycin, yatakemycin, and others (Huang et al., 2012). We sequenced the genome of *Streptomyces* sp. WAC4114 to identify the biosynthetic gene cluster (BGC), with the expectation that the genetic capacity to synthesize the duocarmycin warhead may be absent.

Surprisingly, this was not the case. Bioinformatic analysis of the sequenced genome using antiSMASH (Blin et al., 2019) identified a BGC highly similar to that of CC-1065, including orthologous genes required for warhead assembly. The only notable absences from the *Streptomyces* sp. WAC4114 BGC were orthologs of *c10R1*, a predicted AraC family regulator, and *c10R6*, related to GyrI/SbmC, a gyrase inhibitory protein that protects *E. coli* from microcin B17 (Romanowski et al., 2002) (Figure 3A). The latter gene, *c10R6*, has been characterized as a cyclopropanoid cyclopropyl hydrolase, catalyzing the hydrolysis of the cyclopropyl warhead of CC-1065 and yatakemycin, likely conferring self-resistance (Yuan et al., 2017). Its absence suggests that *Streptomyces* sp. WAC4114 either supports a secondary means of resistance to CC-1065 or does not produce significant quantities of the toxic compound under standard growth conditions.

Consistent with the absence of the putative resistance gene, we did not detect CC-1065 production in *Streptomyces* sp.

WAC4114. To confirm the biosynthesis of PDE-I_2 from this cluster, we captured the BGC into an integrative *Streptomyces* vector using yeast-mediated transformation associated recombination cloning (Tang et al., 2015); the resulting vector, pWAC4114, was introduced by conjugation into the heterologous expression strains *S. coelicolor* M1146 and *S. coelicolor* M1154. Mobilization of pWAC4114 into *S. coelicolor* M1146 and M1154 yielded no exconjugants, suggesting that CC-1065 may be produced in the heterologous background, resulting in cell death.

To circumvent potential CC-1065 toxicity and verify the production of PDE-I_2 in the heterologous expression system, the rSAM-encoding gene required for installation of the cyclopropane warhead, *orf19*, was deleted from pWAC4114 using λ-red mediated recombination (Gust et al., 2003). The resulting construct, pWAC4114Δ*orf19*, supported PDE-I_2 production in *S. coelicolor* M1146 and M1154 (Figures 3B and 3C). Together, these results suggest that, despite what appears to be a functional CC-1065 BGC, *Streptomyces* sp. WAC4114 may downregulate warhead synthesis during the final stages of CC-1065 production, leading to the accumulation of the PDE-I_2 shunt product detected in our antimalarial screen (Figure 3D).

PDE-I_2 is a nanomolar inhibitor of parasite schizogony, inhibiting cytokinesis

The antiplasmodial activities of purified PDE-I_2, duocarmycin TM (a synthetic analog of duocarmycin [Howard et al., 2002], shown in Figure S1A and hereafter referred to as duocarmycin), and chloroquine were tested against a *P. falciparum* canonical reference strain (3D7) and a multidrug-resistant strain (7G8) in our proliferation assay. In parallel, PDE-I_2, duocarmycin, and two control compounds, the DHFR inhibitor WR99210 (Fidock et al., 1998) and the casein kinase 2 inhibitor CX4945 (Ruiz-Carrillo et al., 2018), were tested against a panel of human cell lines in proliferation and cell viability assays. PDE-I_2 was highly potent against both drug-sensitive and multidrug-resistant *P. falciparum* parasites with IC_{50} values between 20 nM and 30 nM. Inhibition of human cell proliferation was only observed in the range of 20 to 50 μM (viability 4–30 μM), an approximately 1,000-fold higher concentration (Figures 4A and 4B, Table S2). As expected, with an intact warhead, duocarmycin was proportionally >1,000-fold more active in both *Plasmodium* and human cell lines. Lacking an alkylating group, we postulated that PDE-I_2 should cause less DNA damage to human cells than a duocarmycin family compound, even at proportionally cytotoxic concentrations. To address this possibility, we performed comet assays in HEK cells treated with PDE-I_2, duocarmycin, or the alkylating agent MMS (using their IC_{90} values). As expected, PDE-I_2 was significantly less genotoxic than duocarmycin (Figure 4C).

To analyze stage-specific inhibition of parasite proliferation, a tightly synchronized culture was treated at the ring stage (3 hpi) with IC_{50} and IC_{90} concentrations of PDE-I_2. PDE-I_2-treated *P. falciparum* cultures showed no difference in parasite development compared with the control within the first 32 hours; however, at 40 hpi, treated parasites were arrested in schizont stages (Figures 4D and 4E, S1B). Notably, duocarmycin treatment led to an indistinguishable arrest (Figures 4E and S1C). PDE-I_2-arrested parasites showed severe impairment of nuclei formation leading to an amorphic degenerated late-stage parasite (Figure 5A). Given the compound's activity at the schizont stage, when DNA replication and nuclear division are at their peaks, coupled with direct observation of conferred defects in nuclei formation, we explored whether the PDE-I_2-induced phenotype in *P. falciparum* may result from impaired DNA replication in the parasite. Flow cytometric analysis of PDE-I_2-treated parasites showed a reduction in the DNA content compared with the control, on par with duocarmycin, the DHFR inhibitor WR99210, and the DNA polymerase inhibitor aphidicolin (Figure 5A).

Given that PDE-I_2-treated parasites are unable to form segmented schizonts (Figures 4C and 4D, S1), we further investigated the effects of PDE-I_2 on distinct elements of cytokinesis, namely MTOC (microtubule-organizing center) organization, secretory organelle biogenesis, inner membrane complex (IMC) formation and parasite plasma membrane (PPM) invagination. In *P. falciparum*, MTOCs anchor mitotic spindles to the nuclear membrane and are accordingly critical to downstream events of cellular division (Francia and Striepen, 2014; Francia et al., 2015). Tubulin staining confirmed the presence of MTOCs in both PDE-I_2-treated and control parasites (Figure 5B); however, the number of MTOCs in PDE-I_2-treated parasites was significantly reduced compared with the control (Figure 5B).

Rhoptries and the IMC are both Golgi-derived structures that are formed *de novo* during schizogony. While the IMC is a double-membrane structure beneath the plasma membrane with primary function in cell motility and architecture (Ferreira et al., 2020), the rhoptries are secretory organelles that serve as storage compartments for secreted proteins that play a pivotal role in host cell invasion (Harding and Frischknecht, 2020). IMC forms in a polar fashion, initiating proximal to the MTOC and extends to surround the nascent daughter parasites. Subsequently, the PPM invaginates, forming a layer covering the IMC (Scheme 1). To visualize these structures, we used three transgenic parasite lines expressing the rhoptry protein PfARO (*armadillo repeats only* [Cabrera et al., 2012]), the IMC protein GAPM2 (*glideosome-associated protein with multiple membrane spans 2* [Bullen et al., 2009; Kono et al., 2012]), or the PPM-associated protein PfSMS1 (Sphingomyelin synthase 1) (Kono et al., 2016) as mCherry or GFP fusion proteins (Figures 5C–5E). We show that while PDE-I_2-treated parasites can form rhoptries visible as punctate foci in mature schizonts, their number was significantly reduced (Figure 5C); however, the most significant defects conferred by PDE-I_2 treatment were observed in IMC and PPM formation and organization. While IMC biogenesis is initiated, no subsequent growth along the nascent daughter cells' polar axis could be observed (Figures 5D and S2A). PDE-I_2 treatment also severely impaired PPM formation (Figures 5E and S2B). This result is in line with previous work that established an association of IMC maturation and PPM invagination (Kono et al., 2016). We examined a more limited set of markers in the context of duocarmycin, and found consistent defects in nuclei formation and IMC biogenesis (Figure S2C).

Both PDE-I_2 and duocarmycins are genotoxic to malaria and exert their effects during actively replicating stages of parasite growth

To address the underlying cause of the schizont arrest, we performed time-of-addition studies with PDE-I_2; duocarmycin; the

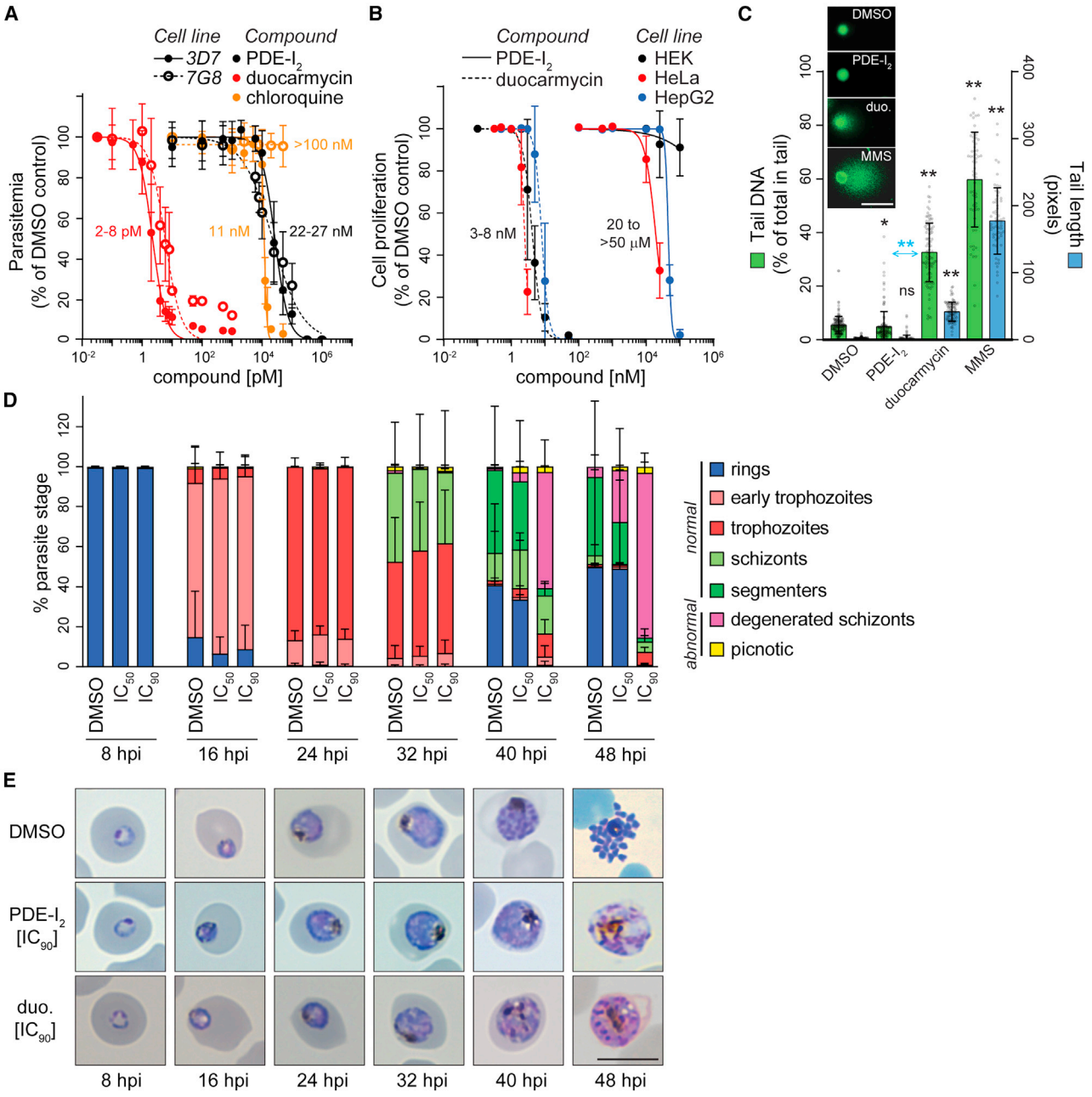

Figure 4. PDE-I_2 is potent, non-toxic, and active in a stage-specific manner against *P. falciparum*

(A and B) Dose-response curves against *P. falciparum* (A) and various mammalian cell lines (B). Data points represent mean ± SD of triplicates from three independent experiments. Range of IC_{50} values across one or more strain/line for a given compound are indicated adjacent to the curves.

(C) Comet assays in HEK cells. Compounds were tested at IC_{90} values determined for HEK cells (PDE-I_2; duocarmycin) or 750 µM MMS. Representative comets for each treatment are shown in the inset panel. Bar graphs represent mean ± SD of n(DMSO) = 184; n(PDE-I_2) = 140; n(duocarmycin) = 97; n(MMS) = 58 obtained from two biological replicates. Significance was tested using the Kruskal-Wallis non-parametric test, with multiple hypothesis testing (Dunn), as compared with the DMSO control. ns, not significant; *$p < 0.001$; **$p < 0.0001$. PDE-I_2 and duocarmycin treatment was compared using the Mann-Whitney non-parametric test (2-tailed). Blue arrow, **$p < 0.0001$. Scale bar, 50 µm.

(D) Stage-specific activity of PDE-I_2 against *P. falciparum*. Bar graphs represent quantification of parasite stages counted every 8 hours in Giemsa-stained blood smears of synchronized *P. falciparum* 3D7 cultures after treatment with compound PDE-I_2 (IC_{50}/IC_{90}) at 3 hpi. Percentages represent mean ± SD from three independent experiments. For all time points, a total number of at least 1,000 parasites were counted by two different researchers.

(E) Representative images of parasite stages after treatment with PDE-I_2 or duocarmycin (IC_{90}) at 3 hpi. Images were taken every 8 hours. Scale bar, 8 µm. See also Table S1 and Figure S1.

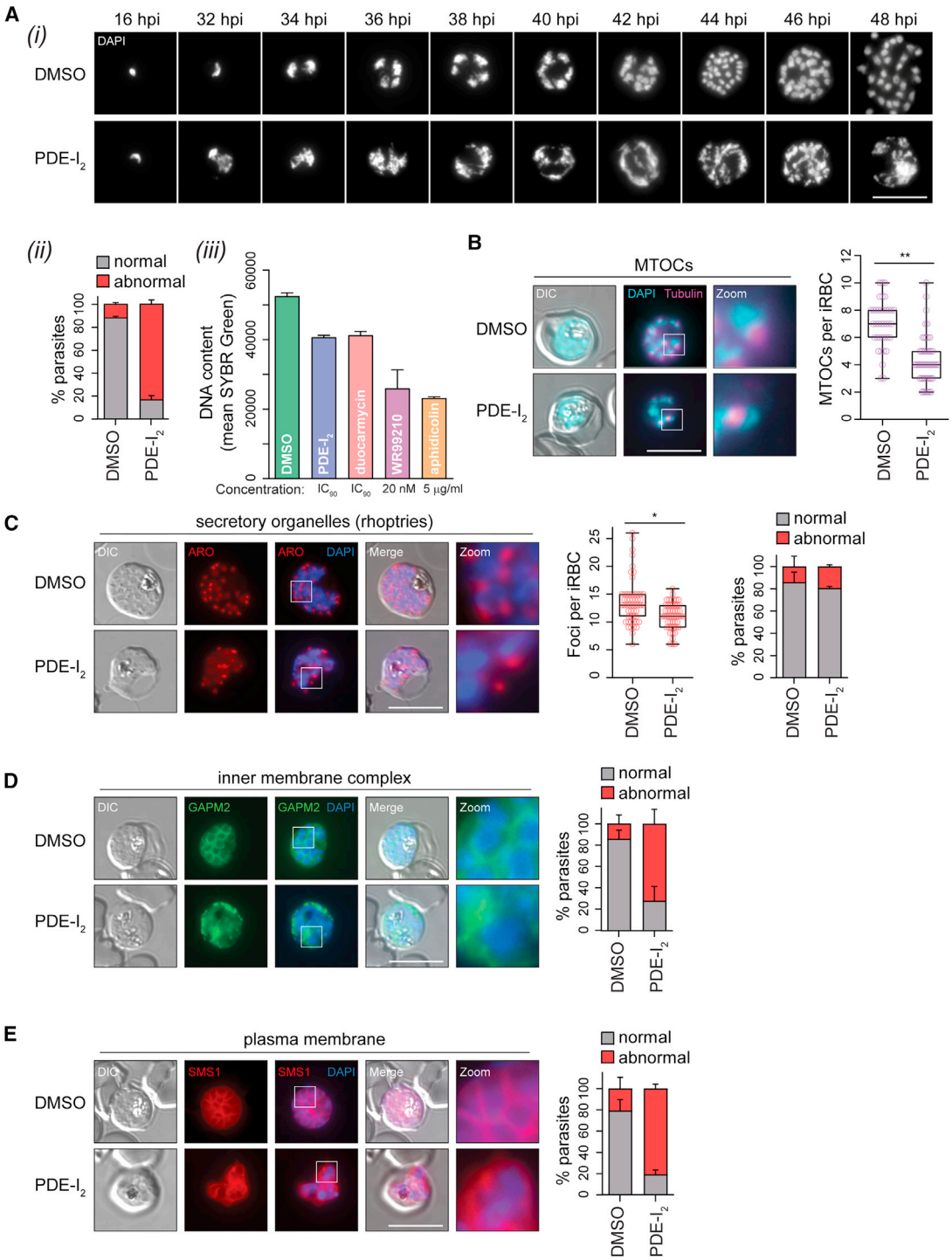

Figure 5. PDE-I_2 inhibits the formation of nuclei and daughter merozoites

(A) *(i)* The morphology of nuclei was analyzed by fluorescence microscopy of DAPI-stained wild-type (3D7) parasites at different time points (16–48 hpi). *(ii)* Bar graph represents percentage of parasites with normal versus abnormal morphology of the nucleus at 48 hpi. In total, at least 400 parasites were analyzed per condition. *(iii)* Bar graph represents DNA content of parasites measured by flow cytometry based on SYBR Green DNA staining. Data points represent mean ± SEM of two biological replicates. Per replicate, at least 100,000 events were recorded.

(B) MTOCs were analyzed by tubulin staining (Tubulin Tracker Deep Red, Thermo Fisher Scientific). Box plot represents number of MTOCs per parasite at 40 hpi. n(DMSO) = 38; n(PDE-I_2) = 48.

(C) The morphology of rhoptries was analyzed by fluorescence microscopy of ARO-mCherry at 48 hpi. Box plot represents number of mCherry-foci per parasite at 48 hpi. n(DMSO) = 53; n(PDE-I_2) = 50. Bar graph represents percentage of parasites with normal versus abnormal morphology of rhoptries. In total, at least 180 parasites were analyzed per condition.

(legend continued on next page)

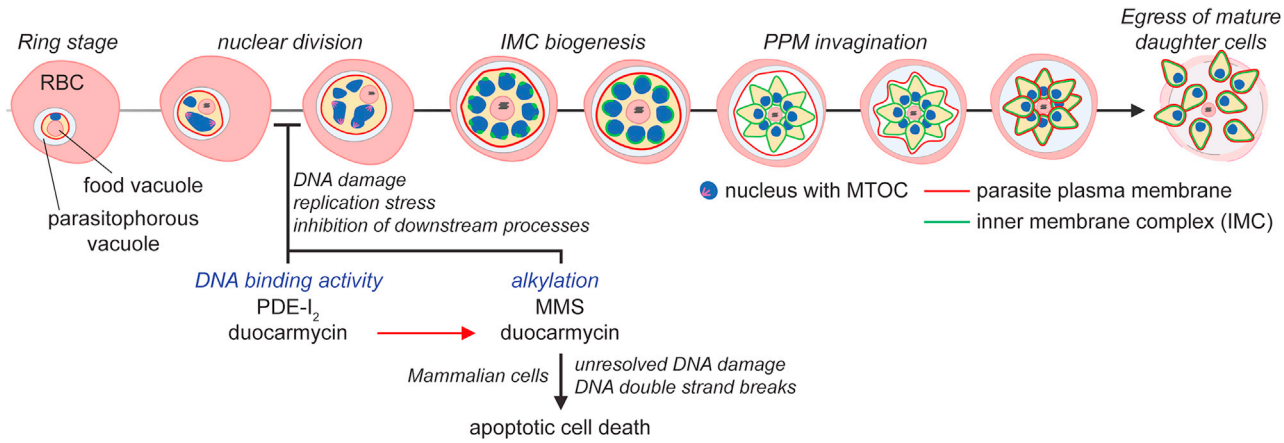

Scheme 1. Schematic of the events of schizogony

The inferred point of action of PDE-I_2 is indicated. Duocarmycins utilize a two-step mechanism, DNA binding and DNA alkylation. Both affect schizogony, while only the latter step appears to cause significant DNA breakage in mammalian cells. Created with BioRender.com.

alkylating agent MMS; compounds causing replication arrest (WR99210, aphidicolin); or compound 2, a protein kinase inhibitor that causes a defect in membrane breakdown and egress at the segmenter stage (Donald et al., 2006). Compounds were added at times preceding (4 hpi), during (24 hpi), or after the majority of DNA replication had completed (40 hpi) and parasites were imaged at 8-hour intervals (Figures 6A-B, S3 and S4). All compounds examined conferred a similar arrest when added prior to completion of DNA replication (Figure S3). In contrast, only compound 2 was able to arrest parasites when added at 40 hpi; all other compounds triggered parasite arrest at the end of the next cycle of infection. We quantitated the morphological features of parasites treated with each compound and found PDE-I_2- and duocarmycin-treated parasites to be indistinguishable (Figures 6B and S4B). In contrast, while the replication inhibitors WR99210 and aphidicolin shared the same temporal requirements of compound addition, their morphological features were distinct, characterized by formation of large vacuoles. MMS-treated parasites exhibited features intermediate between PDE-I_2 or duocarmycin and replication inhibitors.

To further establish an association between DNA metabolism and the phenotypic effects of PDE-I_2 or duocarmycin, we examined the effect of these compounds in the context of non-replicating sexual gametocyte development (Figures 6C and S5). Sexual gametocyte stages were cultivated using a *P. falciparum* NF54 inducible gametocyte producer (iGP) line (Boltryk et al., 2021). Gametocytes maturate over characteristic developmental stages (stage I to stage V, Figure 6C) before being taken up by a mosquito; subsequently, parasites are activated by altered pH and temperature, and the presence of xanthurenic acid in the milieu of the mosquito midgut. Upon activation, gametocytes lose their characteristic shape and "round up." Male gametocytes (making up ~20% of the gametocyte population) undergo three rounds of genomic replication before they exflagellate for fertilization of a female gamete. Activation of stage V gametocytes *in vitro* was stimulated by incubation at room temperature in the presence of xanturenic acid (Figure 6C). Inhibitors of DNA replication, WR99210 and aphidicolin, were included as controls. CX4945 ("Silmitasertib"), an inhibitor of casein kinase 2 (Ruiz-Carrillo et al., 2018), a kinase that has been demonstrated to be essential for gametocyte maturation (Hitz et al., 2021), was included as a positive control. With the exception of CX4945, neither replication inhibitors nor duocarmycin/PDE-I_2 affected gametocyte development. In contrast, all compounds impaired DNA replication when day 11 parasites (enriched for stage V, with the exception of CX4945-treated cells) were activated to round up, suggesting the lack of a phenotype was not due to reductions in compound uptake, as has been observed in gametocytes (Figure 6C) (Bouyer et al., 2020; Saul et al., 1990).

Finally, given the temporal and developmental association between DNA replication and the phenotypic effects of PDE-I_2 and duocarmycin, we examined whether, in contrast to the case for mammalian cells, we could observe an effect of PDE-I_2 on parasite chromosome stability in comet assays (Figure 6D). Surprisingly, duocarmycin and PDE-I_2 conferred comparable damage to *P. falciparum*.

Together, these results suggest that in the context of malaria, the duocarmycin warhead contributes to the potency of the molecules only, while the DNA binding specificity, shared between PDE-I_2 and duocarmycin, is sufficient to confer mode-of-action and selectivity between human and malarial cells (Scheme 1).

(D) Formation of the IMC was analyzed by fluorescence microscopy of GAPM2-GFP at 48 hpi. Bar graph represents percentage of parasites with normal versus abnormal morphology of IMC. In total, at least 150 parasites were analyzed per condition.

(E) Invagination of the PPM was analyzed by fluorescence microscopy of SMS1-mCherry at 48 hpi. Bar graph represents percentage of parasites with normal versus abnormal morphology of PPM. In total, at least 250 parasites were analyzed per condition. All assays were performed with highly synchronous parasites (2-hour synchronicity window) incubated with IC_{90} of PDE-I_2 or vehicle (DMSO) at 2 hpi. The final DMSO concentration did not exceed 0.5%. Scale bars, 8 μM; DIC = differential interference contrast. Nuclei were stained with DAPI. White squares indicate magnified sections shown in the rightmost image of each panel. All bar graphs represent means of two (A) or three (C–F) biological replicate experiments. Error bars represent SEM (A) or SD (C–E). Box plots are derived from three biological replicates (B and C). Whiskers represent min/max. Significance was assessed by t test (GraphPad Prism). *$p < 0.001$; **$p < 0.0001$. See also Figure S2.

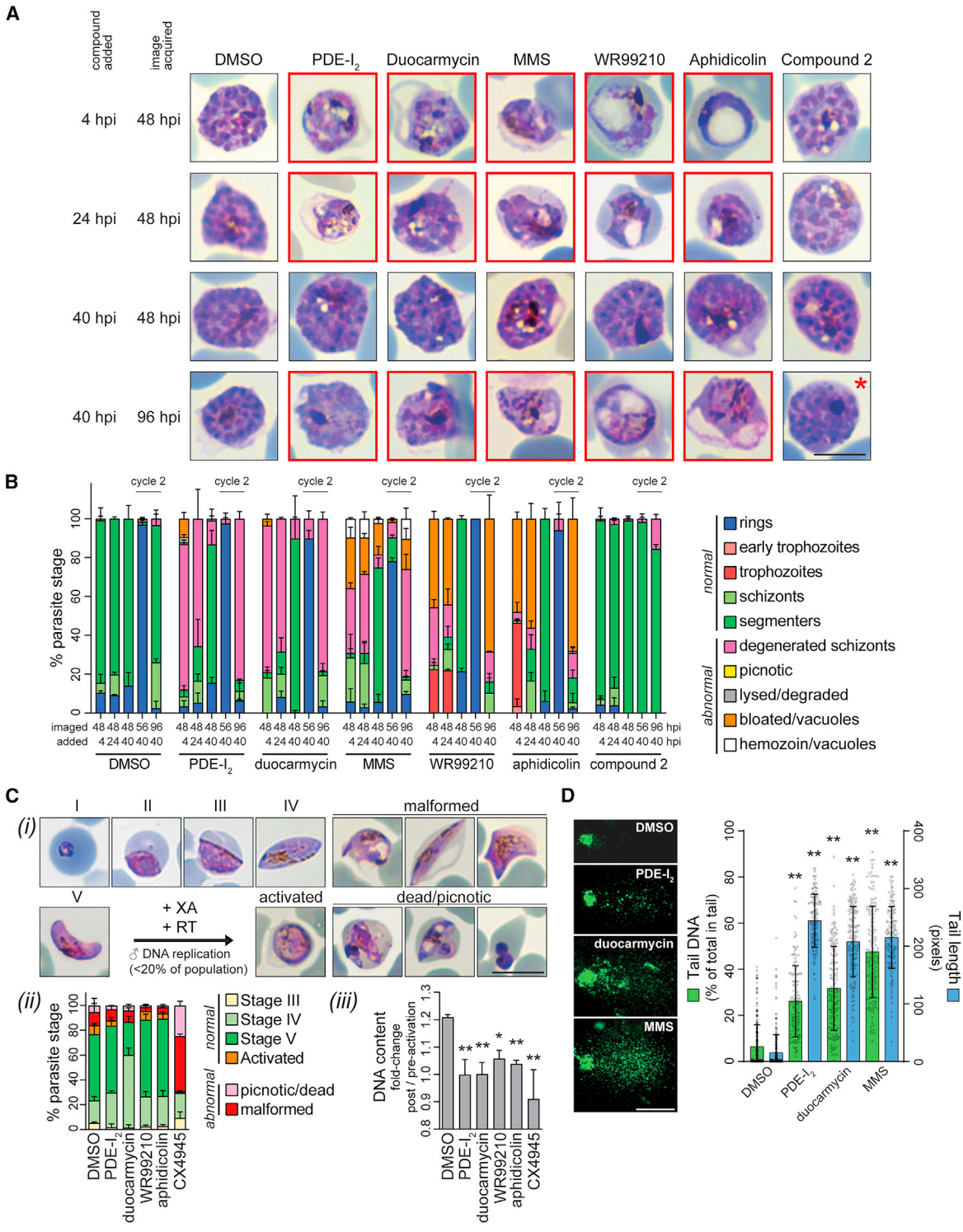

Figure 6. PDE-I_2 impairs DNA replication and causes DNA fragmentation in malaria

(A) Representative images of parasite stages after treatment with PDE-I_2, duocarmycin, or control compounds at 4, 24, or 48 hpi. Images were taken every 8 hours; 48- or 96-hpi images are shown. Examples of abnormal schizonts are indicated by red boxes. Cells treated with compound 2 do not initiate a second cycle, but remain arrested at the segmenter stage (red asterisk). Scale bar, 8 μm.

(B) Bar graphs represent quantification of parasite stages counted every 8 hours in Giemsa-stained blood smears of synchronized *P. falciparum* 3D7 cultures after treatment with the indicated compounds at the indicated times. Select time points are shown. Percentages represent mean ± SEM from two independent experiments. For all time points, a total number of at least 500 parasites were counted.

(legend continued on next page)

DISCUSSION

Given their sub-nanomolar anticancer potency, duocarmycins have been intensely investigated as cancer therapeutics (Jukes et al., 2020). Over the past 40 years, the natural product CC-1065 and multiple synthetic duocarmycin-family derivatives (adozelesin, bizelesin, carzelesin, KW-2189) have been investigated in clinical trials (Cristofanilli et al., 1998; Markovic et al., 2002; Pavlidis et al., 2000; Schwartz et al., 2003). These trials have been discontinued due to lack of efficacy and severe adverse events associated with drug administration. Current efforts center around sophisticated tumor-targeting strategies, using antibody-drug conjugates or prodrug formulations to deliver the toxic duocarmycin-family payload only to sites of tumors (Jukes et al., 2020).

As with their application in cancer therapy, the concept of deploying duocarmycins as antimalarials is not a new one. Duocarmycins specifically target AT-rich sequences, and the genome of *P. falciparum* is extremely AT-rich (~80%) (Weber, 1987). Many previous studies have sought to leverage this property, demonstrating the antimalarial potential of duocarmycin and synthetic analogs (CC-1065, U-71184, tafuramycin, adozelesin, bizelesin, centanamycin) (Chavda et al., 2010; Kiakos et al., 2018; Lee and Inselburg, 1993; Purcell et al., 2008a; Woynarowski et al., 2007; Yanow et al., 2006, 2008). Unfortunately, these compounds share the same liability in the context of malaria as they do in cancer; they are simply too toxic (Jukes et al., 2020). Next-generation tumor-targeting duocarmycins may yet prove efficacious in cancer, though these cancer-specific strategies have left malaria behind.

A significant reason for the extreme toxicity of duocarmycins is readily evident when considering the mechanism of action. Not only do these compounds bind to DNA (MacMillan and Boger, 2009), but they are also chemically reactive, further damaging it by alkylation (Hurley et al., 1988). In mammalian cells, the reactive cyclopropyl duocarmycin warhead enables covalent adduct formation with DNA. This alkylation stalls DNA replication forks and activates the DNA damage checkpoint (Liu et al., 2003; Wang et al., 2001), leading to apoptotic cell death (Cao et al., 2003). Unsurprisingly, given the mechanism of action, the presence of the alkylating warhead and the corresponding mutagenicity correlates with the potency of the molecules; analogs lacking the cyclopropyl group are three to four orders of magnitude less active against human cell lines *in vitro* and four to five orders of magnitude less mutagenic (PDE-I_2,/$U_{66,266}$ [Harbach et al., 1988; Hurley et al., 1988]). The cyclopropyl group is also required for activity *in vivo*; a CC-1065 analog lacking the cyclopropyl group is inactive in mouse models of leukemia at the highest doses reported, relative to its cognate molecule (6 mg/kg/d [Hurley et al., 1988]).

Our identification of the duocarmycin precursor PDE-I_2 as an inhibitor of blood-stage malaria proliferation is an unexpected and exciting result that differentiates this compound from the highly toxic alkylating mature natural product. The potency of PDE-I_2 (IC_{50} ~ 20–30 nM) is comparable to antimalarials in the clinic, including drugs like chloroquine (13 nM), artemisinin (11 nM), and pyrimethamine (10 nM) (Baniecki et al., 2007). It is doubtful that we would have predicted PDE-I_2 to be so potent *a priori*, and our discovery emphasizes the value of crude extract phenotype screening.

We note that PDE-I_2 treatment induces an arrest in the schizont stage of development, with severe defects in daughter cell formation. Parasite arrest neither occurs if PDE-I_2 is added after the bulk of DNA replication is complete, nor if it is added to non-replicating gametocytes, similar to other compounds that impair DNA metabolism. Morphologically, PDE-I_2 and duocarmycin have indistinguishable effects on parasites, different from replication inhibitors or the alkylating agent MMS, suggesting that while DNA metabolism may be the primary target, the precise impingement conferred by PDE-I_2 and duocarmycin is distinct.

Adozelesin, a synthetic analog of CC-1065, damages *P. falciparum* DNA *in vitro* (Yanow et al., 2006). Consistently, treating *Plasmodium* sp. parasites with the duocarmycin family analogs adozelesin, centamycin, or tafuramycin A irreversibly sterilizes parasites, forming the basis for chemical attenuation approaches in vaccine development (Good et al., 2013; Purcell et al., 2008a, 2008b; Raja et al., 2016; Reiman et al., 2018). Similarly, we observe DNA damage in parasites treated with either duocarmycin TM or PDE-I_2, despite the latter lacking a cyclopropyl warhead. The defect in DNA segregation and cytokinesis that we observe may represent a terminal response to unresolved genome damage, accumulated during and manifested after replication is complete. Whether this arrest represents an orchestrated checkpoint response or a catastrophic consequence of failures in DNA replication remains to be seen. Interpretation is complicated by a lack of understanding of how checkpoints function in the multinucleated schizonts of *P. falciparum*, if such checkpoints exist at all (Matthews et al., 2018).

The blood stage of malarial proliferation, with multiple rounds of DNA replication and inherent challenges in DNA surveillance and repair, would seem a prime target for DNA damage agents, and yet parasites in this life-cycle stage are not inherently orders of

(C) (*i*) Representative images of sexual gametocyte stages I to V of a *P. falciparum* NF54 gametocyte producer line (iGP, provided by Till Voss, Swiss TPH). Activation of mature stage V gametocytes was induced by treatment with 100 μM xanthurenic acid (XA) at room temperature (RT). Upon activation, male gametocytes (<20% of gametocyte population) round up and undergo three rounds of genomic replication within 15 min. Examples of gametocytes that were classified as malformed or picnotic/dead are shown. (*ii*) Stage quantification on day 11 of gametocyte development after continuous treatment from day one with PDE-I_2, duocarmycin or control compounds. Percentages represent mean ± SEM from two independent experiments. For all time points, a total number of at least 500 parasites were counted. (*iii*) Quantification of DNA content by SYBR Gold staining in stage V gametocytes versus activated stages after treatment as indicated in (*ii*) and activation as described in (*i*). DNA content was quantified by SYBR Gold staining using an EnVision multilabel plate reader (PerkinElmer) and expressed as fold change post/pre-activation. Bar graphs represent mean ± SD of triplicates from two biological replicates. Significance was tested using one-way ANOVA, equal variance, Dunnett's multiple comparison. *$p < 0.001$ versus DMSO; **$p < 0.0001$. Scale bar, 8 μm.

(D) Comet assays in *P. falciparum* cells. Compounds were tested at IC_{90} values determined for *P. falciparum* cells. (Left) Representative comets for each treatment are shown. (Right) Bar graphs represent mean ± SD of n(DMSO) = 271; n(PDE-I_2) = 140; n(duocarmycin) = 169; n(MMS) = 150 obtained from two biological replicates. Significance was tested using the Kruskal-Wallis non-parametric test, with multiple hypothesis testing (Dunn), as compared with the DMSO control. **$p < 0.0001$. Scale bar = 10 μm. All assays were performed with parasites incubated with IC_{90} of PDE-I_2/duocarmycin/MMS/CX4945; 20 nM WR99210; 5 μg/mL aphidicolin; 1 μM compound 2; or vehicle (DMSO). The final DMSO concentration did not exceed 0.5%. See also Figures S3–S5.

magnitude more sensitive than human cells. For instance, while PDE-I_2 and warhead-containing duocarmycins are approximately 1,000-fold selective for malaria, parasites and human cell lines are sensitive to similar levels of MMS (IC_{90} values on the order of 1 mM for both HEK cells and *P. falciparum 3D7*). While our data support a target for both compounds in DNA metabolism, the selectivity could come from another mechanism. The name PDE-I stands for phosphodiesterase inhibitor, as the compound was first identified from *Streptomyces* culture filtrates in a screen against rabbit phosphodiesterase (Enomoto et al., 1978). However, while the genome of *P. falciparum* encodes for four phosphodiesterases (PDEα, PDEβ, PDEγ, PDEδ), only PDEβ appears to be essential for survival of asexual blood stages of the parasite, and it acts at the stage of invasion, not schizogony (Flueck et al., 2019; Lakshmanan et al., 2015; Moon et al., 2009; Schwach et al., 2015; Taylor et al., 2008; Wentzinger et al., 2008; Yuasa et al., 2005; Zhang et al., 2018a). Further, while duocarmycin and PDE-I_2 share a similar DNA binding preference, their core structure differs, suggesting a common secondary protein target would be unlikely (Figures 2 and S1A). The most probable cause of the selectivity of PDE-I_2 and duocarmycin-family compounds, as has been speculated in the literature, is their DNA binding specificity (Woynarowski et al., 2007).

Like CC-1065, the methyl-ester of PDE-I_2 (and the trimeric analog, PDE-I_3) has been demonstrated to bind to and stabilize the minor groove of DNA, selectively for A-T rich sequences (Kd $\sim$ 0.2 μM) (Boger et al., 1990). While CC-1065 protects DNA from modification in footprinting experiments, an analog lacking the cyclopropyl moiety does not (Hurley et al., 1988). Together these results are consistent with PDE-I_2 binding to DNA *in vivo* in a non-covalent fashion. In addition to potential selectivity conferred by the relative AT-content in malaria versus human cells, a compelling target for PDE-I_2 or duocarmycin binding may be the "super-AT islands" within the malarial genome, 2.3- to 2.5-kb regions containing $\sim$97% AT-content; these regions represent the core of each chromosomal centromere (Hoeijmakers et al., 2012; Kelly et al., 2006; Woynarowski et al., 2007). These regions are enriched for duocarmycin family-member binding sites and have been hypothesized to also be sites of nuclear matrix attachment (Woynarowski et al., 2007). It is tempting to speculate that PDE-I_2 binding is enriched in these regions and that this binding, in turn, impairs replication, causes DNA fragmentation, and impairs MTOC formation and the downstream events in daughter cell formation. In this context, it is important to note that the *de novo* synthesis of essential structures, such as IMC, is initiated but not completed and that other replication stresses lead to disruption of schizogony as well.

Regardless of the precise explanation for the selectivity of PDE-I_2, our data demonstrate that the duocarmycin warhead is not required for potent and selective antimalarial activity. This observation opens avenues for malaria-specific SAR on molecules lacking the genotoxic warhead, with opportunities to leverage decades of medicinal chemistry aimed at engineering duocarmycin family scaffolds.

SIGNIFICANCE

Malaria is one of the deadliest infectious diseases on the planet, responsible for 409,000 deaths and 229 million cases in 2019. Parasites of the genus *Plasmodium* are the causative agent, with the species *P. falciparum* responsible for most fatal cases of malaria. The lack of an effective vaccine means mitigating the global burden of malaria relies on antiplasmodial drug treatments, currently centered on ACT. The emergence of resistance to almost all established antiplasmodial drugs emphasizes the urgent need for new drugs with novel modes of action. Here we identify a selective nanomolar inhibitor of blood-stage malarial proliferation from a screen of microbial natural product extracts. We identify PDE-I_2, a non-toxic precursor of the anticancer duocarmycin family. PDE-I_2 retains the class's signature AT-sequence selective DNA binding but lacks its alkylating cyclopropyl warhead. Despite this difference, PDE-I_2 induces genotoxic stress and severe defects in nuclear segregation in malaria, leading to an impairment of daughter cell formation during schizogony. In the context of malaria, unlike cancer, the cyclopropyl warhead of a duocarmycin family member is dispensable. This discovery identifies a chemotype for further antimalarial drug development and highlights the distinct malarial biology, which is compromised by PDE-I_2. Duocarmycins have been heavily investigated as anticancer therapeutics, with multiple analogs entering clinical trials, which have been discontinued due to toxicity. While duocarmycins are also potent antimalarials, these observations are similarly limited by host toxicity. Building from the PDE-I_2 scaffold, absent the alkylating warhead, we anticipate that decades of duocarmycin medicinal chemistry can be leveraged to rapidly deploy malaria-specific molecules, lacking the toxicity of their predecessors.

STAR★METHODS

Detailed methods are provided in the online version of this paper and include the following:

- KEY RESOURCES TABLE
- RESOURCE AVAILABILITY
  - Lead contact
  - Materials availability
  - Data and code availability
- EXPERIMENTAL MODEL AND SUBJECT DETAILS
- METHOD DETAILS
  - *P. falciparum* strains and culture
  - Parasite synchronisation
  - HTS screen of parasite proliferation using a microbial NP extract library
  - HEK293T cell viability secondary assay
  - IC_{50} and IC_{90} determination
  - Parasite imaging
  - Flow cytometry
  - Isolation and activity-guided purification of PDE-I_2
  - Genome sequencing of *Streptomyces* sp. WAC4114 and heterologous expression of PDE-I_2
  - Target cloning and heterologous expression of the PDE-I_2 BGC
  - Gene knockout of the rSAM coding gene (*orf19*) in pWAC4114

- Comet assay
- Gametocyte assay

- QUANTIFICATION AND STATISTICAL ANALYSIS

SUPPLEMENTAL INFORMATION

Supplemental information can be found online at https://doi.org/10.1016/j.chembiol.2021.10.005.

ACKNOWLEDGMENTS

This research was funded by a Canadian Institutes of Health Research grant (FRN-148463), the Ontario Research Fund, and by a Canada Research Chair to G.D.W.; and a Canadian Institutes for Health Research grant (MOP# 111196), Joachim Hertz Foundation Project grant, Partnership of Universität Hamburg and DESY (PIER) to T.W.G. A.A. received a scholarship from the Jürgen Manchot Foundation. Parts of the graphical abstract and Scheme 1 were created using BioRender (www.BioRender.com).

AUTHOR CONTRIBUTIONS

A.A., N.S., M.X., M.A.C., T.W.G., and G.D.W. conceptualized the study; A.A. and N.S. developed the methodology; A.A., N.S., M.X., J.W.J., W.W., M.A.C., T.W.G., and G.D.W. validated the study; A.A., N.S., W.W., and M.A.C. performed the formal analysis; A.A., N.S., M.X., J.W.J., W.W., D.P., J.R., and S.L. performed study investigation; A.A., M.X., M.A.C., T.W.G., and G.D.W. wrote the original draft; all authors reviewed and edited the article; A.A., N.S., M.X., J.W.J., and M.A.C. performed visualization; T.W.G. and G.D.W. supervised the study; A.A., T.W.G., and G.D.W. performed project administration; and T.W.G. and G.D.W. acquired the funding.

DECLARATION OF INTERESTS

The authors declare no competing interests.

Received: April 29, 2021
Revised: August 15, 2021
Accepted: October 2, 2021
Published: October 27, 2021

REFERENCES

Ahmad, S.J., Abdul Rahim, M.B.H., Baharum, S.N., Baba, M.S., and Zin, N.M. (2017). Discovery of antimalarial drugs from streptomycetes metabolites using a metabolomic approach. J. Trop. Med. *2017*, 2189814.

Ashley, E.A., Dhorda, M., Fairhurst, R.M., Amaratunga, C., Lim, P., Suon, S., Sreng, S., Anderson, J.M., Mao, S., Sam, B., et al. (2014). Spread of artemisinin resistance in *Plasmodium falciparum* malaria. N. Engl. J. Med. *371*, 411–423.

Aurrecoechea, C., Brestelli, J., Brunk, B.P., Dommer, J., Fischer, S., Gajria, B., Gao, X., Gingle, A., Grant, G., Harb, O.S., et al. (2009). PlasmoDB: a functional genomic database for malaria parasites. Nucl. Acids Res. *37*, D539–D543.

Baniecki, M.L., Wirth, D.F., and Clardy, J. (2007). High-throughput *Plasmodium falciparum* growth assay for malaria drug discovery. Antimicrob. Agents Chemother. *51*, 716–723.

Bhatt, S., Weiss, D.J., Cameron, E., Bisanzio, D., Mappin, B., Dalrymple, U., Battle, K.E., Moyes, C.L., Henry, A., Eckhoff, P.A., et al. (2015). The effect of malaria control on *Plasmodium falciparum* in Africa between 2000 and 2015. Nature *526*, 207–211.

Blin, K., Shaw, S., Steinke, K., Villebro, R., Ziemert, N., Lee, S.Y., Medema, M.H., and Weber, T. (2019). antiSMASH 5.0: updates to the secondary metabolite genome mining pipeline. Nucl. Acids Res. *47*, W81–W87.

Boger, D.L., and Coleman, R.S. (1988). Total synthesis of (+)-CC-1065 and ent-(-)-CC-1065. J. Am. Chem. Soc. *110*, 1321–1323.

Boger, D.L., and Johnson, D.S. (1995). CC-1065 and the duocarmycins: unraveling the keys to a new class of naturally derived DNA alkylating agents. Proc. Natl. Acad. Sci. U S A *92*, 3642–3649.

Boger, D.L., Invergo, B.J., Coleman, R.S., Zarrinmayeh, H., Kitos, P.A., Thompson, S.C., Leong, T., and McLaughlin, L.W. (1990). A demonstration of the intrinsic importance of stabilizing hydrophobic binding and non-covalent van der Waals contacts dominant in the non-covalent CC-1065/B-DNA binding. Chem. Biol. Interact. *73*, 29–52.

Boltryk, S.D., Passecker, A., Alder, A., Carrington, E., van de Vegte-Bolmer, M., van Gemert, G.-J., van der Starre, A., Beck, H.-P., Sauerwein, R.W., Kooij, T.W.A., et al. (2021). CRISPR/Cas9-engineered inducible gametocyte producer lines as a valuable tool for *Plasmodium falciparum* malaria transmission research. Nat. Commun. *12*, 4806.

Bouyer, G., Barbieri, D., Dupuy, F., Marteau, A., Sissoko, A., N'Dri, M.-E., Neveu, G., Bedault, L., Khodabux, N., Roman, D., et al. (2020). *Plasmodium falciparum* sexual parasites regulate infected erythrocyte permeability. Commun. Biol. *3*, 726.

Bullen, H.E., Tonkin, C.J., O'Donnell, R.A., Tham, W.-H., Papenfuss, A.T., Gould, S., Cowman, A.F., Crabb, B.S., and Gilson, P.R. (2009). A novel family of Apicomplexan glideosome-associated proteins with an inner membrane-anchoring role. J. Biol. Chem. *284*, 25353–25363.

Burkot, T.R., Williams, J.L., and Schneider, I. (1984). Infectivity to mosquitoes of *Plasmodium falciparum* clones grown in vitro from the same isolate. Trans. R. Soc. Trop. Med. Hyg. *78*, 339–341.

Cabrera, A., Herrmann, S., Warszta, D., Santos, J.M., John Peter, A.T., Kono, M., Debrouver, S., Jacobs, T., Spielmann, T., Ungermann, C., et al. (2012). Dissection of minimal sequence requirements for rhoptry membrane targeting in the malaria parasite. Traffic *13*, 1335–1350.

Cao, P., McHugh, M.M., Melendy, T., and Beerman, T. (2003). The DNA minor groove-alkylating cyclopropylpyrroloindole drugs adozelesin and bizelesin induce different DNA damage response pathways in human colon carcinoma HCT116 cells. Mol. Cancer Ther. *2*, 651–659.

Carter, P., Fitzjohn, S., Halazy, S., and Magnus, P. (1987). Studies on the synthesis of the antitumor agent CC-1065. Synthesis of PDE I and PDE II, inhibitors of cyclic adenosine-3',5'-monophosphate phosphodiesterase using the 3,3'-bipyrrole strategy. J. Am. Chem. Soc. *109*, 2711–2717.

Chavda, S., Babu, B., Yanow, S.K., Jardim, A., Spithill, T.W., Kiakos, K., Kluza, J., Hartley, J.A., and Lee, M. (2010). A novel achiral seco-cyclopropylpyrido[e]indolone (CPyl) analog of CC-1065 and the duocarmycins: synthesis, DNA interactions, in vivo anticancer and anti-parasitic evaluation. Bioorg. Med. Chem. *18*, 5016–5024.

Chatterjee, A.K., and Yeung, B.K.S. (2012). Back to the future: lessons learned in modern target-based and whole-cell lead optimization of antimalarials. Curr. Top. Med. Chem. *12*, 473–483.

Cowman, A.F., Healer, J., Marapana, D., and Marsh, K. (2016). Malaria: biology and disease. Cell *167*, 610–624.

Cristofanilli, M., Bryan, W.J., Miller, L.L., Chang, A.Y., Gradishar, W.J., Kufe, D.W., and Hortobagyi, G.N. (1998). Phase II study of adozelesin in untreated metastatic breast cancer. Anticancer. Drugs *9*, 779–782.

Datsenko, K.A., and Wanner, B.L. (2000). One-step inactivation of chromosomal genes in Escherichia coli K-12 using PCR products. Proc. Natl. Acad. Sci. U S A *97*, 6640–6645.

Donald, R.G.K., Zhong, T., Wiersma, H., Nare, B., Yao, D., Lee, A., Allocco, J., and Liberator, P.A. (2006). Anticoccidial kinase inhibitors: identification of protein kinase targets secondary to cGMP-dependent protein kinase. Mol. Biochem. Parasitol. *149*, 86–98.

Enomoto, Y., Furutani, Y., Naganawa, H., Hamada, M., Takeuchi, T., and Umezawa, H. (1978). Isolation and characterization of PDE-I and II, the inhibitors of cyclic adenosine-3′,5′-monophosphate phosphodiesterase. Agric. Biol. Chem. *42*, 1331–1336.

Ferreira, J.L., Heincke, D., Wichers, J.S., Liffner, B., Wilson, D.W., and Gilberger, T.-W. (2020). The dynamic roles of the inner membrane complex in the multiple stages of the malaria parasite. Front. Cell. Infect. Microbiol. *10*, 611801.

Fidock, D.A., Nomura, T., and Wellems, T.E. (1998). Cycloguanil and its parent compound proguanil demonstrate distinct activities against *Plasmodium falciparum* malaria parasites transformed with human dihydrofolate reductase. Mol. Pharmacol. *54*, 1140–1147.

Francia, M.E., and Striepen, B. (2014). Cell division in apicomplexan parasites. Nat. Rev. Microbiol. *12*, 125–136.

Flueck, C., Drought, L.G., Jones, A., Patel, A., Perrin, A.J., Walker, E.M., Nofal, S.D., Snijders, A.P., Blackman, M.J., and Baker, D.A. (2019). Phosphodiesterase beta is the master regulator of cAMP signalling during malaria parasite invasion. PLoS Biol *17*, e3000154.

Francia, M.E., Dubremetz, J.-F., and Morrissette, N.S. (2015). Basal body structure and composition in the apicomplexans Toxoplasma and Plasmodium. Cilia *5*, 3.

Gamo, F.-J., Sanz, L.M., Vidal, J., de Cozar, C., Alvarez, E., Lavandera, J.-L., Vanderwall, D.E., Green, D.V.S., Kumar, V., Hasan, S., et al. (2010). Thousands of chemical starting points for antimalarial lead identification. Nature *465*, 305–310.

Gaur, A.H., McCarthy, J.S., Panetta, J.C., Dallas, R.H., Woodford, J., Tang, L., Smith, A.M., Stewart, T.B., Branum, K.C., Freeman, B.B., 3rd, et al. (2020). Safety, tolerability, pharmacokinetics, and antimalarial efficacy of a novel *Plasmodium falciparum* ATP4 inhibitor SJ733: a first-in-human and induced blood-stage malaria phase 1a/b trial. Lancet Infect. Dis. *20*, 964–975.

Gomez-Escribano, J.P., and Bibb, M.J. (2011). Engineering streptomyces coelicolor for heterologous expression of secondary metabolite gene clusters. Microb. Biotechnol. *4*, 207–215.

Good, M.F., Reiman, J.M., Rodriguez, I.B., Ito, K., Yanow, S.K., El-Deeb, I.M., Batzloff, M.R., Stanisic, D.I., Engwerda, C., Spithill, T., et al. (2013). Cross-species malaria immunity induced by chemically attenuated parasites. J. Clin. Invest. *123*, 3353–3362.

Guiguemde, W.A., Shelat, A.A., Bouck, D., Duffy, S., Crowther, G.J., Davis, P.H., Smithson, D.C., Connelly, M., Clark, J., Zhu, F., et al. (2010). Chemical genetics of *Plasmodium falciparum*. Nature *465*, 311–315.

Guiguemde, W.A., Shelat, A.A., Garcia-Bustos, J.F., Diagana, T.T., Gamo, F.-J., and Guy, R.K. (2012). Global phenotypic screening for antimalarials. Chem. Biol. *19*, 116–129.

Gust, B., Challis, G.L., Fowler, K., Kieser, T., and Chater, K.F. (2003). PCR-targeted Streptomyces gene replacement identifies a protein domain needed for biosynthesis of the sesquiterpene soil odor geosmin. Proc. Natl. Acad. Sci. U S A *100*, 1541–1546.

Harbach, P.R., Zimmer, D.M., Mazurek, J.H., and Bhuyan, B.K. (1988). Mutagenicity of the antitumor antibiotic CC-1065 and its analogues in mammalian (V79) cells and bacteria. Cancer Res. *48*, 32–36.

Harding, C.R., and Frischknecht, F. (2020). The riveting cellular structures of apicomplexan parasites. Trends Parasitol. *36*, 979–991.

Hitz, E., Grüninger, O., Passecker, A., Wyss, M., Scheurer, C., Wittlin, S., Beck, H.-P., Brancucci, N.M.B., and Voss, T.S. (2021). The catalytic subunit of *Plasmodium falciparum* casein kinase 2 is essential for gametocytogenesis. Commun. Biol. *4*, 336.

Hoeijmakers, W.A.M., Flueck, C., Françoijs, K.-J., Smits, A.H., Wetzel, J., Volz, J.C., Cowman, A.F., Voss, T., Stunnenberg, H.G., and Bártfai, R. (2012). *Plasmodium falciparum* centromeres display a unique epigenetic makeup and cluster prior to and during schizogony. Cell. Microbiol. *14*, 1391–1401.

Howard, T.T., Lingerfelt, B.M., Purnell, B.L., Scott, A.E., Price, C.A., Townes, H.M., McNulty, L., Handl, H.L., Summerville, K., Hudson, S.J., et al. (2002). Novel furano analogues of duocarmycin C1 and C2: design, synthesis, and biological evaluation of seco-iso-cyclopropylfurano[2,3-e]indoline (seco-iso-CFI) and seco-cyclopropyltetrahydrofurano[2,3-f]quinoline (seco-CFQ) analogues. Bioorg. Med. Chem. *10*, 2941–2952.

Huang, W., Xu, H., Li, Y., Zhang, F., Chen, X.-Y., He, Q.-L., Igarashi, Y., and Tang, G.-L. (2012). Characterization of yatakemycin gene cluster revealing a radical S-adenosylmethionine dependent methyltransferase and highlighting spirocyclopropane biosynthesis. J. Am. Chem. Soc. *134*, 8831–8840.

Hurley, L.H., Lee, C.S., McGovren, J.P., Warpehoski, M.A., Mitchell, M.A., Kelly, R.C., and Aristoff, P.A. (1988). Molecular basis for sequence-specific DNA alkylation by CC-1065. Biochemistry *27*, 3886–3892.

Johnson, J.D., Dennull, R.A., Gerena, L., Lopez-Sanchez, M., Roncal, N.E., and Waters, N.C. (2007). Assessment and continued validation of the malaria SYBR green I-based fluorescence assay for use in malaria drug screening. Antimicrob. Agents Chemother. *51*, 1926–1933.

Jukes, Z., Morais, G.R., Loadman, P.M., and Pors, K. (2020). How can the potential of the duocarmycins be unlocked for cancer therapy? Drug Discov. Today.

Kelly, J.M., McRobert, L., and Baker, D.A. (2006). Evidence on the chromosomal location of centromeric DNA in *Plasmodium falciparum* from etoposide-mediated topoisomerase-II cleavage. Proc. Natl. Acad. Sci. U S A *103*, 6706–6711.

Kiakos, K., Englinger, B., Yanow, S.K., Wernitznig, D., Jakupec, M.A., Berger, W., Keppler, B.K., Hartley, J.A., Lee, M., and Patil, P.C. (2018). Design, synthesis, nuclear localization, and biological activity of a fluorescent duocarmycin analog. Hxtfa. Bioorg. Med. Chem. Lett. *28*, 1342–1347.

Kieser, T., Bibb, M.J., Buttner, M.J., Chater, K.F., and Hopwood, D.A. (2000). Practical *Streptomyces* Genetics (John Innes Found).

Kono, M., Herrmann, S., Loughran, N.B., Cabrera, A., Engelberg, K., Lehmann, C., Sinha, D., Prinz, B., Ruch, U., Heussler, V., et al. (2012). Evolution and architecture of the inner membrane complex in asexual and sexual stages of the malaria parasite. Mol. Biol. Evol. *29*, 2113–2132.

Kono, M., Heincke, D., Wilcke, L., Wong, T.W.Y., Bruns, C., Herrmann, S., Spielmann, T., and Gilberger, T.W. (2016). Pellicle formation in the malaria parasite. J. Cell Sci. *129*, 673–680.

Lakshmanan, V., Fishbaugher, M.E., Morrison, B., Baldwin, M., Macarulay, M., Vaughan, A.M., Mikolajczak, S.A., and Kappe, S.H.I. (2015). Cyclic GMP balance is critical for malaria parasite transmission from the mosquito to the mammalian host. MBio *6*, e02330.

Lambros, C., and Vanderberg, J.P. (1979). Synchronization of *Plasmodium falciparum* erythrocytic stages in culture. J. Parasitol. *65*, 418–420.

Lee, S., and Inselburg, J. (1993). In vitro sensitivity of *Plasmodium falciparum* to drugs that bind DNA or inhibit its synthesis. J. Parasitol. *79*, 780–782.

Liu, J.-S., Kuo, S.-R., Beerman, T.A., and Melendy, T. (2003). Induction of DNA damage responses by adozelesin is S phase-specific and dependent on active replication forks. Mol. Cancer Ther. *2*, 41–47.

MacMillan, K.S., and Boger, D.L. (2009). Fundamental relationships between structure, reactivity, and biological activity for the duocarmycins and CC-1065. J. Med. Chem. *52*, 5771–5780.

MacNeil, D.J., Gewain, K.M., Ruby, C.L., Dezeny, G., Gibbons, P.H., and MacNeil, T. (1992). Analysis of *Streptomyces avermitilis* genes required for avermectin biosynthesis utilizing a novel integration vector. Gene *111*, 61–68.

Malleret, B., Claser, C., Ong, A.S.M., Suwanarusk, R., Sriprawat, K., Howland, S.W., Russell, B., Nosten, F., and Rénia, L. (2011). A rapid and robust tri-color flow cytometry assay for monitoring malaria parasite development. Sci. Rep. *1*, 118.

Markovic, S.N., Suman, V.J., Vukov, A.M., Fitch, T.R., Hillman, D.W., Adjei, A.A., Alberts, S.R., Kaur, J.S., Braich, T.A., Leitch, J.M., et al. (2002). Phase II trial of KW2189 in patients with advanced malignant melanoma. Am. J. Clin. Oncol. *25*, 308–312.

Matthews, H., Duffy, C.W., and Merrick, C.J. (2018). Checks and balances? DNA replication and the cell cycle in *Plasmodium*. Parasit. Vectors *11*, 216.

Moon, R.W., Taylor, C.J., Bex, C., Schepers, R., Goulding, D., Janse, C.J., Waters, A.P., Baker, D.A., and Billker, O. (2009). A cyclic GMP signalling module that regulates gliding motility in a malaria parasite. PLoS Pathog *5*, e1000599.

Noskov, V.N., Kouprina, N., Leem, S.-H., Ouspenski, I., Barrett, J.C., and Larionov, V. (2003). A general cloning system to selectively isolate any eukaryotic or prokaryotic genomic region in yeast. BMC Genomics *4*, 16.

Ostling, O., and Johanson, K.J. (1984). Microelectrophoretic study of radiation-induced DNA damages in individual mammalian cells. Biochem. Biophys. Res. Commun. *123*, 291–298.

Pan, W.-H., Xu, X.-Y., Shi, N., Tsang, S.W., and Zhang, H.-J. (2018). Antimalarial activity of plant metabolites. Int. J. Mol. Sci. *19, 1382*.

Parrish, J.P., Kastrinsky, D.B., Wolkenberg, S.E., Igarashi, Y., and Boger, D.L. (2003). DNA alkylation properties of yatakemycin. J. Am. Chem. Soc. *125*, 10971–10976.

Pavlidis, N., Aamdal, S., Awada, A., Calvert, H., Fumoleau, P., Sorio, R., Punt, C., Verweij, J., van Oosterom, A., Morant, R., et al. (2000). Carzelesin phase II study in advanced breast, ovarian, colorectal, gastric, head and neck cancer, non-Hodgkin's lymphoma and malignant melanoma: a study of the EORTC early clinical studies group (ECSG). Cancer Chemother. Pharmacol. *46*, 167–171.

Plouffe, D.M., Wree, M., Du, A.Y., Meister, S., Li, F., Patra, K., Lubar, A., Okitsu, S.L., Flannery, E.L., Kato, N., et al. (2016). High-Throughput assay and discovery of small molecules that interrupt malaria transmission. Cell Host Microbe *19*, 114–126.

Purcell, L.A., Yanow, S.K., Lee, M., Spithill, T.W., and Rodriguez, A. (2008a). Chemical attenuation of *Plasmodium berghei* sporozoites induces sterile immunity in mice. Infect. Immun. *76*, 1193–1199.

Purcell, L.A., Wong, K.A., Yanow, S.K., Lee, M., Spithill, T.W., and Rodriguez, A. (2008b). Chemically attenuated *Plasmodium sporozoites* induce specific immune responses, sterile immunity and cross-protection against heterologous challenge. Vaccine *26*, 4880–4884.

Raja, A.I., Cai, Y., Reiman, J.M., Groves, P., Chakravarty, S., McPhun, V., Doolan, D.L., Cockburn, I., Hoffman, S.L., Stanisic, D.I., et al. (2016). Chemically attenuated blood-stage plasmodium yoelii parasites induce long-lived and strain-transcending protection. Infect. Immun. *84*, 2274–2288.

Reiman, J.M., Kumar, S., Rodriguez, I.B., Gnidehou, S., Ito, K., Stanisic, D.I., Lee, M., McPhun, V., Majam, V., Willemsen, N.M., et al. (2018). Induction of immunity following vaccination with a chemically attenuated malaria vaccine correlates with persistent antigenic stimulation. Clin. Transl. Immunol. *7*, e1015.

Rivadeneira, E.M., Wasserman, M., and Espinal, C.T. (1983). Separation and concentration of schizonts of *Plasmodium falciparum* by Percoll gradients. J. Protozool. *30*, 367–370.

Romanowski, M.J., Gibney, S.A., and Burley, S.K. (2002). Crystal structure of the *Escherichia coli* SbmC protein that protects cells from the DNA replication inhibitor microcin B17. Proteins *47*, 403–407.

Rottmann, M., McNamara, C., Yeung, B.K.S., Lee, M.C.S., Zou, B., Russell, B., Seitz, P., Plouffe, D.M., Dharia, N.V., Tan, J., et al. (2010). Spiroindolones, a potent compound class for the treatment of malaria. Science *329*, 1175–1180.

Ruiz-Carrillo, D., Lin, J., El Sahili, A., Wei, M., Sze, S.K., Cheung, P.C.F., Doerig, C., and Lescar, J. (2018). The protein kinase CK2 catalytic domain from *Plasmodium falciparum*: crystal structure, tyrosine kinase activity and inhibition. Sci Rep *8*, 7365.

Saul, A., Graves, P., and Edser, L. (1990). Refractoriness of erythrocytes infected with *Plasmodium falciparum* gametocytes to lysis by sorbitol. Int. J. Parasitol. *20*, 1095–1097.

Schwach, F., Bushell, E., Gomes, A.R., Anar, B., Girling, G., Herd, C., Rayner, J.C., and Billker, O. (2015). PlasmoGEM, a database supporting a community resource for large-scale experimental genetics in malaria parasites. Nucleic Acids Res *43*, D1176–82.

Schwartz, G.H., Patnaik, A., Hammond, L.A., Rizzo, J., Berg, K., Von Hoff, D.D., and Rowinsky, E.K. (2003). A phase I study of bizelesin, a highly potent and selective DNA-interactive agent, in patients with advanced solid malignancies. Ann. Oncol. Off. J. Eur. Soc. Med. Oncol. *14*, 775–782.

Singh, N.P., McCoy, M.T., Tice, R.R., and Schneider, E.L. (1988). A simple technique for quantitation of low levels of DNA damage in individual cells. Exp. Cell Res. *175*, 184–191.

Smilkstein, M., Sriwilaijaroen, N., Kelly, J.X., Wilairat, P., and Riscoe, M. (2004). Simple and inexpensive fluorescence-based technique for high-throughput antimalarial drug screening. Antimicrob. Agents Chemother. *48*, 1803–1806.

Spangenberg, T., Burrows, J.N., Kowalczyk, P., McDonald, S., Wells, T.N.C., and Willis, P. (2013). The open access malaria box: a drug discovery catalyst for neglected diseases. PLoS One *8*, e62906.

Sun, W., Huang, X., Li, H., Tawa, G., Fisher, E., Tanaka, T.Q., Shinn, P., Huang, W., Williamson, K.C., and Zheng, W. (2017). Novel lead structures with both *Plasmodium falciparum* gametocytocidal and asexual blood stage activity identified from high throughput compound screening. Malar. J. *16*, 147.

Tang, X., Li, J., Millán-Aguiñaga, N., Zhang, J.J., O'Neill, E.C., Ugalde, J.A., Jensen, P.R., Mantovani, S.M., and Moore, B.S. (2015). Identification of thiotetronic acid antibiotic biosynthetic pathways by target-directed genome mining. ACS Chem. Biol. *10*, 2841–2849.

Taylor, C.J., McRobert, L., and Baker, D.A. (2008). Disruption of a *Plasmodium falciparum* cyclic nucleotide phosphodiesterase gene causes aberrant gametogenesis. Mol. Microbiol. *69*, 110–118.

Trager, W., and Jensen, J.B. (1976). Human malaria parasites in continuous culture. Science *193*, 673–675.

Van Voorhis, W.C., Adams, J.H., Adelfio, R., Ahyong, V., Akabas, M.H., Alano, P., Alday, A., Alemán Resto, Y., Alsibaee, A., Alzualde, A., et al. (2016). Open source drug discovery with the malaria box compound collection for neglected diseases and beyond. PLoS Pathog. *12*, e1005763.

Walliker, D., Quakyi, I.A., Wellems, T.E., McCutchan, T.F., Szarfman, A., London, W.T., Corcoran, L.M., Burkot, T.R., and Carter, R. (1987). Genetic analysis of the human malaria parasite *Plasmodium falciparum*. Science *236*, 1661–1666.

Wang, Y., Beerman, T.A., and Kowalski, D. (2001). Antitumor drug adozelesin differentially affects active and silent origins of DNA replication in yeast checkpoint kinase mutants. Cancer Res. *61*, 3787–3794.

Weber, J.L. (1987). Analysis of sequences from the extremely A + T-rich genome of *Plasmodium falciparum*. Gene *52*, 103–109.

Wells, T.N.C. (2011). Natural products as starting points for future anti-malarial therapies: going back to our roots? Malar. J. *10*, S3.

Wentzinger, L., Bopp, S., Tenor, H., Klar, J., Brun, R., Beck, H.P., and Seebeck, T. (2008). Cyclic nucleotide-specific phosphodiesterases of *Plasmodium falciparum*: PfPDEalpha, a non-essential cGMP-specific PDE that is an integral membrane protein. Int. J. Parasitol. *38*, 1625–1637.

White, N.J., Pukrittayakamee, S., Hien, T.T., Faiz, M.A., Mokuolu, O.A., and Dondorp, A.M. (2014a). Malaria. Lancet (London, England) *383*, 723–735.

White, N.J., Pukrittayakamee, S., Phyo, A.P., Rueangweerayut, R., Nosten, F., Jittamala, P., Jeeyapant, A., Jain, J.P., Lefèvre, G., Li, R., et al. (2014b). Spiroindolone KAE609 for falciparum and vivax malaria. N. Engl. J. Med. *371*, 403–410.

World Health Organization. (2020). World Malaria Report: 20 Years of Global Progress and Challenges.

Woynarowski, J.M., Krugliak, M., and Ginsburg, H. (2007). Pharmacogenomic analyses of targeting the AT-rich malaria parasite genome with AT-specific alkylating drugs. Mol. Biochem. Parasitol. *154*, 70–81.

Wu, S., Jian, X.-H., Yuan, H., Jin, W.-B., Yin, Y., Wang, L.-Y., Zhao, J., and Tang, G.-L. (2017). Unified biosynthetic origin of the benzodipyrrole subunits in CC-1065. ACS Chem. Biol. *12*, 1603–1610.

Yanow, S.K., Purcell, L.A., and Spithill, T.W. (2006). The A/T-specific DNA alkylating agent adozelesin inhibits *Plasmodium falciparum* growth in vitro and protects mice against Plasmodium chabaudi adami infection. Mol. Biochem. Parasitol. *148*, 52–59.

Yanow, S.K., Purcell, L.A., Pradel, G., Sato, A., Rodriguez, A., Lee, M., and Spithill, T.W. (2008). Potent antimalarial and transmission-blocking activities of centanamycin, a novel DNA-binding agent. J. Infect. Dis. *197*, 527–534.

Yuan, H., Zhang, J., Cai, Y., Wu, S., Yang, K., Chan, H.C.S., Huang, W., Jin, W.-B., Li, Y., Yin, Y., et al. (2017). Gyrl-like proteins catalyze cyclopropanoid hydrolysis to confer cellular protection. Nat. Commun. *8*, 1485.

Yuasa, K., Mi-Ichi, F., Kobayashi, T., Yamanouchi, M., Kotera, J., Kita, K., and Omori, K. (2005). PfPDE1, a novel cGMP-specific phosphodiesterase from the human malaria parasite *Plasmodium falciparum*. Biochem. J. *392*, 221–229.

Zhang, J.H., Chung, T.D., and Oldenburg, K.R. (1999). A simple statistical parameter for use in evaluation and validation of high throughput screening assays. J. Biomol. Screen. *4*, 67–73.

Zhang, M., Wang, C., Otto, T.D., Oberstaller, J., Liao, X., Adapa, S.R., Udenze, K., Bronner, I.F., Casandra, D., Mayho, M., et al. (2018a). Uncovering the essential genes of the human malaria parasite *Plasmodium falciparum* by saturation mutagenesis. Science *360*.

Zhang, S., Zhu, J., Zechel, D.L., Jessen-Trefzer, C., Eastman, R.T., Paululat, T., and Bechthold, A. (2018b). New WS9326A derivatives and one new annimycin derivative with antimalarial activity are produced by *Streptomyces asterosporus* DSM 41452 and its mutant. Chembiochem *19*, 272–279.

STAR★METHODS

KEY RESOURCES TABLE

REAGENT or RESOURCE	SOURCE	IDENTIFIER
Bacterial and virus strains		
Streptomyces sp. WAC4114	Wright *Actinomycetes* Collection	N/A
Streptomyces coelicolor M1146	(Gomez-Escribano and Bibb, 2011)	N/A
Streptomyces coelicolor M1154	(Gomez-Escribano and Bibb, 2011)	N/A
Escherichia coli BW25113	(Datsenko and Wanner, 2000)	N/A
Escherichia coli top10	Thermo Fisher	Cat. No. C404010
Escherichia coli ET12567	(MacNeil et al., 1992)	N/A
Chemicals, peptides, and recombinant proteins		
SYBR Green	Invitrogen	Cat. No. S7563
SYBR Gold	Invitrogen	Cat. No. S11494
Dihydorethidium	Cayman	Cat. No. 12013
DAPI	Cayman	Cat. No. 14285
TubulinTracker Deep Red	Invitrogen	Cat. No. T34077
PrestoBlue® Cell Viability Agent	Invitrogen	Cat. No. A113261
FOA	Cedarlane	Cat. No. F-230-2.5
PDE-I_2	This manuscript	N/A
Duocarmycin TM	MedChemExpress	Cat. No. HY-107769
Methyl methanesulfonate	Merck	Cat. No. 820775
Chloroquine	Merck	Cat. No. 14194
WR99210	Jacobus Pharmaceuticals	N/A
Aphidicolin	Sigma	Cat. No. A4487
Casein kinase 2 inhibitor (CX4945)	SYNKINASE	Cat. No. SYN-1109
Compound 2	Mike Blackman, The Francis Crick Institute, UK	N/A
D-(+)-Glucosamine	Sigma	Cat. No. G1514
N-Acetyl-D-glucosamine	Roth	Cat. No. 8993.4
Xanthurenic acid	Sigma	Cat. No. D120804
Percoll	GE Healthcare	Cat. No. 17-0891-02
Sorbitol	Sigma	Cat. No. 6213.1
Saponin Quillaja sp.	Sigma	Cat. No. S4521
RPMI 1640 (Gibco)	ThermoFisher	Cat. No. 31800089
AlbuMAX II (Gibco)	ThermoFisher	Cat. No. 11021045
Giemsa's azur eosin methylene blue solution	Merck	Cat. No. 1092040500
Penicillin/Streptomycin	PAN Biotech	Cat. No. P06-07100
Deposited data		
NMR data of the compound PDE-I_2, see Table S1	This manuscript	N/A
Genome sequence, WAC4114	This manuscript	GenBank: PRJNA754115
GraphPad Prism data for Figures 4, 5, and 6 and associated Supplemental Figures/Tables	This manuscript	Mendeley Data: https://doi.org/10.17632/srjnx7dcmp.1
Experimental models: cell lines		
Plasmodium falciparum 3D7	(Walliker et al., 1987)	N/A
Plasmodium falciparum 7G8	(Burkot et al., 1984)	N/A
Plasmodium falciparum 3D7 transgenic cell line: episomal expression of PfSMS1-mCherry	(Kono et al., 2016)	N/A
Plasmodium falciparum 3D7 knock in cell line: GAPM2-GFP (C-terminal GFP-tagging of PfGAPM2)	(Kono et al., 2012)	N/A

(*Continued on next page*)

Continued

REAGENT or RESOURCE	SOURCE	IDENTIFIER
Plasmodium falciparum 3D7 transgenic cell line: episomal expression of PfARO-mCherry	(Cabrera et al., 2012)	N/A
Plasmodium falciparum NF54 knock in cell line: inducible gametocyte producer (iGP) (C-terminal tagging of PfGDV1 with active GlmS ribozyme in the 3' UTR)	(Boltryk et al., 2021)	N/A
HEK293T cells	BNITM, Hamburg, Germany	N/A
HeLa cells	Institute Pasteur, Paris, France	N/A
HepG2 cells	European cell culture collection	N/A
Experimental models: organisms/strains		
Saccharomyces cerevisiae VL6-48N	(Noskov et al., 2003)	N/A
Oligonucleotides		
See Table S2	N/A	N/A
Recombinant DNA		
pWAC4114-koorf19	This manuscript	N/A
pWAC4114	This manuscript	N/A
pKD3	(Datsenko and Wanner, 2000)	N/A
pKD46	(Datsenko and Wanner, 2000)	N/A
pR9406	David Figurski	N/A
pCAP03-aac(3)IV	(Tang et al., 2015)	N/A
Software and algorithms		
BioRender	N/A	https://www.BioRender.com
CometScore 2.0	TriTek Corp.	https://www.RexHoover.com
PlasmoDB	(Aurrecoechea et al., 2009)	https://plasmodb.org/plasmo/
Leica Application Suite X	Leica	https://www.leica-microsystems.com/products/microscope-software/p/leica-las-x-ls/
ChemDraw 20.1.1.125	PerkinElmer	https://perkinelmerinformatics.com/products/research/chemdraw/
Graphpad Prism 6	Graphpad software	https://www.graphpad.com/scientific-software/prism/
AdobePhotoshop CS2	Adobe Systems	https://www.adobe.com/
Adobe Illustrator CS6	Adobe Systems	https://www.adobe.com/
Other		
0+ red blood cells (transfusion blood)	Blood bank University Medical Center Hamburg-Eppendorf (UKE), Germany	N/A
AB+ human blood serum	Centre for Clinical Transfusion Medicine Tuebingen, Germany	N/A
Low melting point agarose	Roth	Cat. No. A4018
Accutase Cell Detachment Solution	PAN Biotech	Cat. No. P10-21100
Tryptic soy broth (TSB)	Fisher Scientific	Cat. No. DF0370-17-3
Yeast extract	Fisher Scientific	Cat. No. BP1422-2
DMEM	PAN Biotech	Cat. No. P04-03500
Fetal Bovine Serum	PAN Biotech	Cat. No. P30-3305
DPBS	PAN Biotech	Cat. No. P04-361000

RESOURCE AVAILABILITY

Lead contact

Further information and requests for resources and reagents should be directed to and will be fulfilled by the lead contact, Gerard Wright (wrightge@mcmaster.ca).

Materials availability

Requests for materials should be made via the lead contact.

Data and code availability

Sequencing data have been deposited at GenBank and are publicly available as of the data of publication. The Bioproject ID is listed in the key resources table. Raw data used to generate plots and bar graphs in Figures 4, 5, and 6, S1, S2, S4, and S5, and Table S2 have been deposited as GraphPad Prism files at Mendeley and are publicly available as of the date of publication. The DOI is listed in the key resources table. Microscopy data reported in this paper will be shared by the lead contact upon request.

This paper does not report original code.

Any additional information required to reanalyze the data reported in this paper is available from the lead contact upon request.

EXPERIMENTAL MODEL AND SUBJECT DETAILS

Streptomyces species and *Saccharomyces cerevisiae* were grown at 30°C, with shaking at 250 rpm for liquid cultures, unless otherwise noted. *Escherichia coli* strains were grown at 37°C with shaking at 250 rpm for liquid cultures. Human cell lines were grown at 37°C without shaking, at 5% CO2. *Plasmodium falciparum* strains were grown at 37°C without shaking, at 5% CO_2; 1%O_2; 94% N_2. Further details on culture conditions are provided in the method details.

METHOD DETAILS

Chemicals and laboratory reagents were laboratory standard grade or above and purchased from Fisher, Roth, or Sigma unless otherwise noted.

P. falciparum strains and culture

Parasites analyzed in this study were cultured in O+ human erythrocytes at 37°C under standard conditions (Trager and Jensen, 1976) in RPMI supplemented with 0.5% AlbuMAX. Parasitemia was monitored by Giemsa-staining of methanol-fixed blood smears. Parasitemia was maintained at a maximum of 10% and culture media was replaced at least every 48 hr. The parasite strains 3D7 (Walliker et al., 1987) and 7G8 (Burkot et al., 1984) (resistant to CQ, PYR, CYC) were used in this study. Other cell lines used in this study were: 3D7 PfARO-mCherry (Cabrera et al., 2012), 3D7 PfGAPM2-GFP (Kono et al., 2012), 3D7 PfSMS1-mCherry (Kono et al., 2016), and an NF54 inducible gametocyte producer (iGP) line (Boltryk et al., 2021).

Parasite synchronisation

To obtain highly synchronous parasite cultures, mature schizont stages were isolated from a 10 mL parasite culture (approx. 5% parasitemia) using 60% Percoll as previously described (Rivadeneira et al., 1983). Isolated schizonts were washed once with RPMI and mixed with 300 μL RBCs and 200 μL RPMI medium in a 1.5 mL reaction tube. Parasites were incubated with shaking (600 rpm) at 37°C for 30 min, transferred to a Petri dish containing 5 mL RPMI medium, and cultured under standard conditions for a further 1.5 hr to allow parasites to egress and reinvade. Subsequently, infected red blood cells were pelleted at 800 xg for 3 min and unruptured schizonts were lysed by incubation with 5 times the volume of 5% sorbitol in PBS. Cells were washed once with RPMI medium and taken back into culture. The resulting parasite culture contained young ring stages with a 2 hr synchronicity window.

HTS screen of parasite proliferation using a microbial NP extract library

Stock cultures of *P. falciparum* 3D7 were synchronized twice with 5% sorbitol as described previously (Lambros and Vanderberg, 1979). Parasite proliferation assays were performed as described (Smilkstein et al., 2004) with slight modifications. In brief, tightly synchronous parasite cultures were seeded as early ring stages (0-14 hpi) into solid sterile black flat bottom 96 well plates (Corning) at a final volume of 200 μL per well at 2% hematocrit and 0.5% parasitemia. Natural products from the Wright Actinomycete Collection (WAC) were stored in DMSO and screened in duplicate for their antimalarial activity. Non-infected erythrocytes in the absence of compound served as a background control, whereas parasite culture with a final concentration of 1 μM chloroquine served as a control for parasite death (positive control). Parasite culture in the absence of compound served as a control for parasite growth (negative control). 0.5% DMSO was included in the untreated positive control. Supernatant (100 μL) was replaced with 100 μL of 1x SYBR Gold stain (Invitrogen) in lysis buffer (20 mM Tris-HCl pH 7.5; 5 mM EDTA, 0.008% saponin; 0.08% Triton-X-100) after 72 hr. The plates were wrapped in foil and freeze/thawed. Final parasitemia was determined by quantification of DNA using a fluorescent nucleic acid intercalating dye, SYBR Gold (Johnson et al., 2007; Smilkstein et al., 2004). Fluorescence was determined using an EnVision multilabel plate reader by PerkinElmer at 485-nm excitation and 535-nm emission wavelengths. All pipetting steps were performed using a Janus Automated workstation (PerkinElmer). Data points were plotted in Graphpad Prism, normalized to DMSO control wells and IC_{50} values calculated from dose-response-curves generated by nonlinear regression. Assay quality was determined by the Z' statistical test (Zhang et al., 1999).

HEK293T cell viability secondary assay

A counterscreen of the NP extract library against HEK293T cells was performed to identify non-specific, toxic hits. HEK293T cells were cultured in Dulbecco Modified Eagle Medium (DMEM) supplemented with 10% fetal bovine serum and 1% Pen/Strep (final

concentration of 100 U/mL penicillin and 100 μg/mL streptomycin). For the assay, 120 cells per well were seeded into 384 well plates and the supernatant replaced after 24 hr with fresh DMEM containing a final concentration of 2% extract. Plates were incubated for a further 48 hr, after which the supernatant was removed and 200 μL 10% PrestoBlue® Cell Viability Agent (Invitrogen) in PBS was added. Cells were incubated for 5 hr at 37°C. Absorbance was measured at 570-600 nm in an EnVision multilabel plate reader (PerkinElmer, integration time 0.1 sec/well). Final DMSO concentration in HEK293T culture was 1%. Wells containing only 1% DMSO served as a negative control. Data points were plotted in Graphpad Prism, normalized to the DMSO control and IC_{50} values were calculated using nonlinear regression.

IC_{50} and IC_{90} determination

Parasite cultures at 0.1% parasitemia and 2% hematocrit were seeded into a solid black flat bottom 96 well plate (200 uL culture per well), incubated with serial dilutions of compound solubilized in DMSO, and cultured under standard conditions (Trager and Jensen, 1976). The final DMSO concentration did not exceed 0.5%. After 96 hr, parasites were lysed and final parasitemia was analyzed by SYBR Gold staining as described above. Data points were plotted in Graphpad Prism, normalized to DMSO control wells, and IC_{50} values were calculated from dose-response-curves generated by nonlinear regression.

Human cells (HEK293T, HepG2, HeLa) were cultured as described above. For IC_{50}/IC_{90}-determination, 2.5 x10^4 cells/well were seeded into a solid black flat bottom 96 well plate (200 μL/well). Cells were incubated at 37°C under 5% CO_2. After 18 hr, the supernatant was removed and fresh DMEM containing serial dilutions of the compounds under investigation were added. Final DMSO concentration in human cell culture was 0.5%. Wells containing 0.5% DMSO served as negative controls. Plates were incubated for a further 48 hr at 37°C under 5% CO_2. To monitor cell viability, the supernatant was removed and cells were incubated with 200 μL 10% PrestoBlue® Cell Viability Agent (Invitrogen) in PBS at 37°C. After 30 min, fluorescence (λ_{ex} = 560 nm, λ_{em} = 590 nm) was measured in an EnVision multilabel plate reader (PerkinElmer, integration time 0.1 sec/well). To monitor proliferation, PrestoBlue-treated cells were washed twice with PBS and incubated with 1x SYBR Gold in lysis solution (20 mM Tris-HCl pH 7.5; 5 mM EDTA, 0.008% saponin; 0.08% Triton-X-100) for 30 min at room temperature in the dark. DNA content was measured in an EnVision multilabel plate reader (PerkinElmer) at 485 nm excitation and 535 nm emission wavelengths. Data points were plotted in Graphpad Prism, normalized to the DMSO control and IC_{50} values were calculated using nonlinear regression.

Parasite imaging

To visualize nuclei, parasites were stained with 1 μg/mL DAPI (Biomol) in RPMI at 37°C for 15 min. Tubulin was stained with 1:1000 Tubulin Tracker™ Deep Red (Thermo Fisher) in RPMI at 37°C for 15 min. For live cell imaging, cells were pelleted at 500 xg for 1 min. The pellet was resuspended in an equal volume of the supernatant, 5 μL of the sample were placed of a microscopy slide and covered with a cover slip. Fluorescence microscopy images were taken with a Leica DM6 B microscope equipped with Leica DFC9000 GT camera using an 100x immersion oil objective. Images were acquired with Leica Application Suite X (LAS X) software and processed using Adobe Photoshop CS2.

Flow cytometry

The DNA content of treated parasites was analyzed by flow cytometry as described previously (Malleret et al., 2011). Resuspended parasite culture (20 μL) was transferred to a 1.5 mL reaction tube and 80 μL RPMI containing SYBR Green (Sigma-Aldrich) and dihydroethidium (DHE, Thermo Fisher). Final concentrations of 0.25x and 5 μg/mL were added, respectively. Samples were incubated for 20 min (protected from light) at room temperature and washed three times with PBS before DNA content was analyzed using a NovoCyte 1000 (ACEA Biosciences Inc.). For every sample at least 100,000 events were recorded.

Isolation and activity-guided purification of PDE-I_2

Streptomyces sp. WAC4114 was grown in 600 mL of Bennett's media in 3 L Fernbach flasks for 6 days at 30°C. Cells were harvested by centrifugation and the conditioned media was extracted with 5% (w/v) HP-20 (Diaion) resin twice (total 10%, w/v). The cell pellets were extracted with acetone (2 x 500 mL) and the extract concentrated under vacuum with 100 g HP-20 resin. The resin fractions were combined and washed with H_2O (1 L), 20% MeOH (2 L), 80% MeOH (2 L), and 100% acetone (3 L) to yield four fractions (Fr1∼ Fr4). The active fraction (Fr4) was dried down and sequentially extracted with hexanes, hexane/ethyl acetate (1:1), and acetone. The active acetone subfraction (Fr4-acetone) was applied to a reverse-phase column (RediSep Rf C18, Teledyne) on a CombiFlash ISCO system. The column was eluted with a water-acetone linear gradient system (5-80% acetone). The active fractions were combined and applied to Sephadex LH-20 column (400 mL) eluting with methanol/acetone (1:1), to yield 1.96 mg PDE-I_2.

Genome sequencing of *Streptomyces* sp. WAC4114 and heterologous expression of PDE-I_2

Streptomyces sp. WAC4114 was grown in TSBY medium (tryptic soy broth, 30 g/L; yeast extract, 5 g/L) at 30°C, 250 rpm, to mid-log phase, and the mycelium was harvested for genomic DNA isolation as previously described (Kieser et al., 2000). Illumina MiSeq sequencing (300 bp, paired end reads) was performed by the McMaster Genomics Facility in the Farncombe Institute at McMaster University. The assembled genome sequence was submitted to antiSMASH (Blin et al., 2019) for secondary metabolite biosynthetic gene cluster analysis.

Target cloning and heterologous expression of the PDE-I_2 BGC

Primers and gBlock used in this study are listed in Table S3. The PDE-I_2 BGC was cloned into the pCAP03-aac(3)IV plasmid using yeast transformation associated recombination as described previously (Tang et al., 2015). pCAP03-aac(3)IV capture vector was digested with *NdeI* and *XhoI* and then assembled with gBlock DNA targetting the boundary sequences of the PDE-I_2 BGC, resulting in pCAP03-4114. pCAP03-4114 was then linearized by *PmeI* digestion and then co-transformed with *AsiSI* digested *Streptomyces* sp. WAC4114 gDNA into *S. cerevisiae* VL6-48N spheroplast cells. Yeast transformants were selected on SD-Trp agar plate supplemented with 5-FOA (1 mg/mL). Plasmid DNA was extracted from yeast transformants for PCR screening, and positive plasmid was then transformed into *E. coli* Top10 cells for propagation followed by restriction mapping analysis. pWAC4114 bearing the PDE-I_2 BGC confirmed by restriction mapping was then re-transformed into *E. coli* ET12567 cells and then mobilized into *S. coelicolor* M1146 and M1154 through *E. coli-Streptomyces* interspecies tri-parental mating using *E. coli* ET12567/pR9406 as the helper strain. The resulting *Streptomyces* exconjugants were examined for heterologous expression.

Gene knockout of the rSAM coding gene (*orf19*) in pWAC4114

orf19 in pWAC4114 was deleted using λ-red mediated PCR-targeting technology (Gust et al., 2003). Primers Δorf19-F/R were used to amplify the *cat* resistance cassette from pKD3, of which two *Avr*II sites were positioned at both sides of *cat* gene. The *cat* cassette was transformed into *E. coli* BW25113/pKD46/pWAC4114 through electroporation, resulting in pWAC4114-Δ*orf19*::*cat*. pWAC4114-Δ*orf19*::*cat* plasmid was then isolated and digested with *Avr*II restriction enzyme overnight at 37°C to remove the *cat* cassette. The digested plasmid was purified by precipitation and then self-ligated using T4 DNA ligase (NEB) to generate the non-scar in-frame deletion mutant of *orf19*, resulting in pWAC4114-Δ*orf19* plasmid. pWAC4114-Δ*orf19* was introduced into *S. coelicolor* M1146 and M1154 strains through tri-parental mating as described above for producing PDE-I_2

Comet assay

For single cell electrophoresis (Ostling and Johanson, 1984; Singh et al., 1988) the protocol of a commercial comet assay kit (EPIDERM^{TM} -201_COMET, MatTek Corporation) was used with slight modifications. For pre-coating, glass slides were dipped into 1% molten agarose in PBS and dried overnight at room temperature.

HEK293T cells (approx. 95% confluence) or *P. falciparum* parasites (5% trophozoites at 20-24 hpi, 5% hematocrit) were treated with potential DNA damaging compounds for 4 hr under standard culture conditions. The final DMSO concentration in the cell culture did not exceed 0.5%.

After compound treatment, HEK293T cells were washed twice with prewarmed PBS and harvested by incubation with Accutase Cell Detachment Solution (PAN Biotech) for 5 min at 37°C. Detached cells were washed twice with PBS and finally resuspended in PBS at a density of approximately 1x 10^6 cells/mL.

P. falciparum parasites were harvested by lysis of red blood cells with 0.01% saponin in ice-cold PBS for 10 min. Parasites were washed three times with ice-cold PBS and finally resuspended in PBS at a density of approximately 1x 10^6 cells/mL.

Cell suspensions were diluted 1:10 in 1% low melting point agarose in PBS (Roth) at 37°C and 75 μL of the sample was pipetted into the middle of precoated glass slide. The sample was covered with a cover slip and incubated at 4°C for 3 min. Before electrophoresis was completed, samples were protected from light at all times. After agarose gelling, the cover slip was gently rotated off by one corner and the slide was immersed in pre-chilled lysis buffer (2.5 M NaCl; 100 mM EDTA; 10 mM Tris; 1% N-lauryl-sarcosine; 1% Triton-X-100, pH 10) at 4°C overnight. After lysis, slides were immersed in pre-chilled unwinding buffer (0.2 N NaOH; 1 mM EDTA, pH 13) at 4°C for 20 min in the dark. Subsequently, slides were placed in an electrophoresis chamber filled with pre-chilled running buffer (0.2 N NaOH; 1 mM EDTA; 1% DMSO, pH 13) and electrophoresis was performed using a constant voltage of 1 Volt/cm (300-350 mA) at 4°C for 30 min. After electrophoresis, slides were neutralized for 10 min in neutralization buffer (400 mM Tris, pH 7.5) at room temperature. Slides were transferred into fresh neutralization buffer and incubated for another 10 min. After neutralization, slides were fixed in 70-95% ethanol for 10 min and dried overnight at room temperature. Samples were stained with SYBR Gold solution (1x in 50 mM Tris, pH 7.5) for 10 min at room temperature, washed once with 50 mM Tris (pH 7.5) for 5 min, and covered with a cover slip. Comets were imaged by epifluorescence microscopy using a Leica DM6 B microscope equipped with Leica DFC9000 GT camera and Leica Application Suite X software. DNA damage was quantified using CometScore 2.0 software (TriTrek Corporation).

Gametocyte assay

Sexual gametocyte stages were produced using a *P. falciparum* NF54 inducible gametocyte producer (iGP) line (Boltryk et al., 2021) allowing targeted overexpression of the sexual commitment factor GDV1 (*Gametocyte Development 1*). NF54 iGP parasites were cultivated under standard conditions in the presence of 2.5 mM glucosamine (GlcN) to inhibit expression of endogenously expressed GlmS ribozyme-tagged GDV1. For induction of sexual commitment, GlcN was removed from the medium of a culture containing 1% ring stages. Parasites were cultured for a further 48 hr under standard conditions in the absence of GlcN to allow reinvasion. After reinvasion, sexual committed rings (day 1) were cultured in RPMI medium supplemented with 0.25% AlbuMAX and 5% human serum (blood group AB+) for 13 days to allow gametocyte maturation. Culture medium was changed daily on a 37°C heating plate and gametocytes were treated with 50 mM N-acetyl-D-glucosamine (GlcNAc) to deplete non-committed asexual stages. Compounds to be tested were directly added to the culture medium from day one of gametocyte maturation. The final DMSO concentration did not exceed 0.5%. Gametocyte morphology was monitored in Giemsa-stained blood smears. For activation, on day 13, mature Stage V gametocytes were treated with 100 μM xanthurenic acid for 20 min at room temperature. DNA content before and after activation

was quantified using SYBR Gold staining. For quantification, 100 μL of the cultures were mixed with an equivalent volume of SYBR Gold staining solution (1x SYBR Gold, 20 mM Tris-HCl pH 7.5; 5 mM EDTA, 0.008% saponin; 0.08% Triton-X-100), transferred into a solid black flat-bottom 96 well plate, and incubated for 30 min at room temperature in the dark. Fluorescence was measured in an EnVision multilabel plate reader (PerkinElmer, integration time 0.1 sec/well). Data was analyzed in Graphpad Prism.

QUANTIFICATION AND STATISTICAL ANALYSIS

In general, data were analyzed and plotted in GraphPad Prism version 6. Dose-response curves were fit using non-linear regression (normalized response - variable slope); 95% confidence intervals for IC_{50} values are indicated in Table S2. Comet assay data were analyzed for statistical significance using the Mann-Whitney non-parametric test or Kruskal-Wallis non-parametric test with Dunnett's multiple comparison (*$p < 0.001$; **$p < 0.0001$). Quantitation of DNA replication in Figure 6C was assessed for statistical significance by one-way ANOVA with equal variance (*$p < 0.001$; **$p < 0.0001$). For each experiment, data points represent mean ± SD or SEM and n represents number of analyzed cells. Boxplots show median with interquartile range, whiskers indicate min to max and statistical analysis was determined by t-test (*$p < 0.001$; **$p < 0.0001$). All assays were performed with two or three biological replicates. p values, exact values of n, details of biological and technical replicates, and data analysis for each experiment can be found in the figure legends.